STUDY ON EXPERIMENTAL CROSS SECTIONS FOR REACTIONS $^{174}Yb(n,\gamma)^{175}Yb$ AND $^{55}Mn(n,\gamma)^{56}Mn$ AT NEW ENERGIES OF 0.0334 AND 0.0536 eV USING NEUTRONS FROM TRIGA NUCLEAR REACTOR

MD. MUSTAFA ZAVED

(*BSc Engg. IIUC*)

A THESIS SUBMITTED FOR THE DEGREE OF MASTER OF ENGINEERING

DEPARTMENT OF NUCLEAR SCIENCE AND ENGINEERING

MILITARY INSTITUE OF SCIENCE AND TECHNOLOGY

2020

The thesis titled **"Study on experimental cross sections for reactions $^{174}Yb(n,\gamma)^{175}Yb$ and $^{55}Mn(n,\gamma)^{56}Mn$ at new energies of 0.0334 and 0.0536 eV using neutrons from TRIGA nuclear reactor"** submitted by Md. Mustafa Zaved, Roll- 1016280002, Session: April, 2016 has been accepted as a satisfactory in partial fulfillment of the requirement for the degree of M.Sc. on Nuclear Science and Engineering.

BOARD OF EXAMINERS

1. Chairman

Dr. Mohammad Amirul Islam
Principal Scientific Officer
Reactor and Neutron Physics Division
INST, AERE, Savar

2. Member

Colonel Md. Rosaidul Mawla, PSC (Ex-Officio)
Head
Department of Nuclear Science and Engineering
MIST, Mirpur, Dhaka

3. Member

Professor Dr. M. A. Rashid Sarkar (Internal)
Professor
Department of Nuclear Science and Engineering
MIST, Mirpur, Dhaka

4. Member

Professor Shaikh Abdul Latif (External)
Nuclear Science and Engineering Department
King Abdul-Aziz University (KAU)
Jeddah, Kingdom of Saudi Arabia

“Declaration

I hereby declare that this thesis is my original work and it has been written by me in its entirety. I have duly acknowledged all the sources of information, which have been used in the thesis. The thesis (fully or partially) has not been submitted for any degree or diploma in any university or institute previously.”

……

Md. Mustafa Zaved

ABSTRACT

The neutron capture cross sections of ^{174}Yb(n,γ)^{175}Yb and ^{55}Mn(n,γ)^{56}Mn reactions at 0.0334 eV and 0.0536 eV energies were experimentally measured for the first time using monochromatic neutrons from a neutron diffractometer and a neutron spectrometer at TRIGA Mark II research reactor. The ^{197}Au$(n,\gamma)^{198}$Au reaction was used as a monitor reaction to determine the neutron beam intensity. High-resolution gamma-ray spectrometry system was used to measure the radioactivity of the product nuclides. After considering all the correction factors such as neutron self-shielding and gamma attenuation effects, the resultant cross sections obtained for the reaction ^{174}Yb(n,γ)^{175}Yb at 0.0334 eV and 0.0536 eV energies are 56.8 ± 3.7 b and 44.2 ± 2.6 b, respectively. The determined experimental values for the reaction at 0.0334 eV and 0.0536 eV are in agreement with the theoretically evaluated data libraries of JENDL-4.0 and ENDF/B-VIII. However, experimentally determined data in this work are around 45% less than the theoretically evaluated JEFF-3.3 data. Similarly, the resultant cross sections obtained for the reaction ^{55}Mn(n,γ)^{56}Mn at 0.0334 eV and 0.0536 eV neutron energies are 11.07±0.60 b and 9.03±0.49 b, respectively. The resultant data for the two reactions were extrapolated to the 0.0253 eV energy by assuming 1/v dependence in the thermal energy region. The extrapolated data at 0.0253 eV for ^{174}Yb(n,γ)^{175}Yb and ^{55}Mn(n,γ)^{56}Mn reactions are 64.8±2.9 b and 12.93±0.99 b, respectively. The data obtained from this study at 0.0253 eV for the reactions are compared with the integrally measured values reported in the literature and different theoretically evaluated data libraries such as ENDF/B-VIII, JENDL-4.0, ROSFOND-2010 and JEFF-3-3. The data obtained from this study at 0.0253 eV for ^{174}Yb(n,γ)^{175}Yb reaction validates the excitation functions of JENDL-4.0 and ENDF/B-VIII data libraries. However, data obtained from this study do not support the JEFF-3-3 data library

at thermal energy region for this reaction. On the other hand, the resultant cross sections for $^{55}Mn(n,\gamma)^{56}Mn$ reaction at 0.0253 eV, 0.0334 eV and 0.0536 eV are consistent with those data libraries within the uncertainty limits. The new cross sectional data obtained from this study are convenient to check the evaluated excitation functions at thermal energy region to resolve discrepancies of the data for the studied reactions which can be used for the proper assessment of the reactor criticality safety. Moreover, the obtained data from this study will also be useful to measure activity distribution, therapeutic radioisotope production and studies related to the interaction of neutrons with matter for the studied targets. This study will also encourage cross-section measurements for various reactions, at different energies in the thermal energy region, at many places in the world where neutron diffractometer and spectrometer are installed.

ACKNOWLEDGEMENT

I would like to express my gratitude, appreciation and indebtedness to my honorable supervisor Dr. Mohammad Amirul Islam, Principal Scientific Officer, Reactor and Neutron Physics Division, Institute of Nuclear Science and Technology (INST), Atomic Energy Research Establishment (AERE), Savar for his enthusiastic guidance and constant encouragement through this research work. I am also grateful to Head, Nuclear Science and Engineering Department of MIST to permit me to carry on this research work. I am indebted to all the faculty members and staffs of my department for their encouragement during my study. I am extremely grateful to Director, INST and Head, RNDP, INST for kindly allowing me to use all the laboratory facilities that I required for my research work. I would like also to express my gratitude to all other officers and staffs of RNPD for their help in conducting the experiments. Finally, I want to express my gratitude to my parents because they were always with me.

TABLE OF CONTENTS

LIST OF SYMBOLS

Abbreviation	Term
NAA	Neutron Activation Analysis
INAA	Instrumental Neutron Activation Analysis
RNAA	Radiochemical Neutron Activation Analysis
PGNAA	Prompt Gamma Ray Neutron Activation Analysis
DGNAA	Delayed Gamma Ray Neutron Activation Analysis
ENAA	Epithermal Neutron Activation Analysis
FNAA	Fast Neutron Activation Analysis
TRIGA	Training, Research, Isotope production General Atomic
TAS	Triple Axis Spectrometer
SAND	Savar Neutron Diffractometer
MCA	Multi Channel Analyzer
HPGe	High Purity Germanium Detector
AERE	Atomic Energy Research Estabilishment
INST	Institute of Nuclear Science and Technology
PTS	Pneumatic Transfer System

TABLE OF FIGURES

LIST OF TABLES

CHAPTER 1

INTRODUCTION

The history of modern nuclear physics starts with the discovery of X-ray by the W. Roentgen in 1895, which created a revolution in the field of physics. In 1896, Henri Becquerel discovered new type of radiation while investigating fluorescence and phosphorescence in uranium salts [1]. Marie Curie and her husband Pierre Curie named this Becquerel radiation of phosphorescence as radioactivity. Today, the nuclear reaction in its broadcast sense is one of the largest field of nuclear physics.

This chapter covers a brief description about basic nuclear properties, neutron induced reactions, importance of neutron absorption cross section, background and present state of the problem and finally objectives of this study.

1.1 Basic Properties of Nuclear Reaction

A nuclear reaction is considered to be the process in which two nuclear particles (two nuclei or a nucleus and a nucleon) interact to produce two or more nuclear particles or gamma rays. Thus, a nuclear reaction must cause a transformation of at least one nuclide to another. The collision or interaction of the incident particle with target is generally described in terms of the cross section. The cross section gives a measure of the probability for a reaction to occur and may be calculated if the form of the basic interaction between the particles is known.

In nuclear reaction, the total energy being the sum of the rest mass energies and kinetics energies of reactants and resulting products is conserved. The energetics of nuclear reaction is determined by the Q value of the reaction. The Q value of the reaction is defined as the

difference between the sum of the masses of the initial reactants and sum of the masses of final products in energy units usually in MeV. If m_y and m_b represents the individual masses of the products and m_a and m_x represents the masses of the reactants, then the Q value is given by

$$Q = \Delta mc^2 = \{(m_a + m_x) - (m_y + m_b)\}\, c^2 \tag{1.1}$$

The mass of an element is expressed in atomic mass unit (amu). One amu is equivalent to 931 MeV. Therefore the equation is

$$Q = \Delta mc^2 = \{(m_a + m_x) - (m_y + m_b)\}\, c^2 \times 931 \text{ MeV} \tag{1.2}$$

If Q is positive, the reaction is exoergic and if Q is negative then the reaction is endoergic.

1.2 Neutron Capture Reaction and Cross-section

Neutrons, discovered in 1932 by Chadwick, are ideal projectiles for inducing nuclear reactions. Neutrons are often captured by stable nuclides. The increase of neutrons in these reactions produces radioactive nuclides, mostly beta emitters. Emission of light particles alpha, beta, and gamma in neutron-induced reactions are often delayed. Half-lives of nuclei produced and their decay energies are determined by experiments, and these data provide identification for the products.

Neutron capture is a kind of nuclear reaction in which an atomic nucleus collides with one or more neutrons and they merge to form a heavier nucleus. As neutrons have no electric charge so they can easily penetrate a nucleus than charged particles, which are repelled by electrostatic repulsion. The probability of the neutron capture by a nucleus is determined by the neutron absorption cross section, which is usually measured in barns (b).The neutron absorption cross section is variable and depends on:

- **Target nucleus** (Hydrogen, Boron, Uranium, etc.). Each isotopes has its own set of cross section.
- **Type of reaction** (Capture, fission, etc.) Cross section is different for each nuclear reaction.
- **Neutron energy** (Thermal, resonance, fast neutron). For a given target and reaction type, the cross section is strongly dependent on the neutron energy. In the common cases, the cross section is usually much larger at low energies than at high energies.
- **Target energy** (Temperature of target material- Doppler broadening). This dependence is not so significant, but the target energy strongly influences inherent safety of nuclear reactors due to a Doppler broadening of resonances.

1.3 Importance of Neutron Capture Cross Section

All the analysis codes for nuclear systems depend on the evaluated cross section data from the nuclear data libraries such as ENDF/BVII or JENDL-3.3. However, the nuclear data found these libraries show discrepancies. Design and analysis of any nuclear system such as reactor core and fuel elements, storage of mixtures of waste with other materials and burned fuel element require high quality nuclear data [2]. Appropriate nuclear data is necessary for reactor design and nuclear criticality calculation. Nuclear data for minor actinides (MAs) and long-lived fission products (LLFs) are necessary for burn up analysis of the nuclear fuels and studies on nuclear transmutation. The nuclear waste problem and the research devoted to new nuclear cycles have triggered a renewed in neutron induced reaction in a wide energy range. The use of incorrect cross section evaluation results in unreliable nuclear criticality calculation. Thus, such problems are one of the major motivations for evaluating new cross section measurement

at different energy especially for the targets having large discrepancies in the cross section data. Moreover, to support the nuclear criticality program, it is important to measure neutron capture cross section over broad energy ranges.

1.4 Background and Present State of the Problem

The investigations of cross sections of neutron induced reactions are of considerable interest, not only for their importance to fundamental research in Nuclear & Reactor Physics and Engineering, but also for practical applications in nuclear technology, dosimetry, radiation safety, improving evaluated nuclear data libraries, etc.

Ytterbium (Yb) is a potential candidate to be used as a neutron absorber in nuclear reactor and used as an alloy material to develop the grain refinement, strength and other mechanical properties of stainless steel to be used for proposed future reactor structure material [3-4]. Among the different isotopes of Yb, thermal neutron capture cross section of ^{174}Yb is of great importance not only for therapeutic radioisotope production of ^{175}Yb by neutron activation method but also for the studies concerning the interaction of neutrons with matter and other fundamental nuclear research [5-7]. On the other hand, Manganese (Mn) is eleventh most abundant element in the earth crust, which has only one stable isotope ^{55}Mn with 100% abundance. In industry, Mn is greatly used, especially in alloying and deoxidizing steel. In nuclear science, the reaction ^{55}Mn(n,γ)^{56}Mn extensively used as a neutron flux monitor since almost from the discovery of the neutron [8]. Manganese (Mn) as a target for (n,γ) reaction is of great interest in neutron transport calculations of nuclear structural material such as nuclear grade stainless steel 304L and 316L which contain 2% of Manganese [9-10]. In a nuclear reactor, neutrons interact with ^{55}Mn present in alloys of nuclear shielding materials and produces radioactive ^{56}Mn having a half-life of 2.8h and emitting main characteristic gamma

ray of 846.8 keV energy. Thus, Mn affects the neutron economy of conventional reactor and advanced heavy water rector [11].

In a nuclear reactor, various energies of neutrons are available. The energy dependence of neutron capture cross sections in a reactor must be well identified for the proper assessment of criticality safety and radiation doses [12]. Presently, it is very much important to measure the neutron capture cross section for most nuclides accurately for the proper calculation of neutron transport, assessments of nuclear reactor safety, investigations of high-burn-up core characteristics, decay heat power predictions and for nuclear transmutation studies. However, most of the thermal neutron capture cross sections in the available compiled data libraries for most of the targets are often provided at the average thermal neutron energy value of 0.0253 eV. The available neutron capture cross section data of the $^{174}Yb(n,\gamma)^{175}Yb$ reaction at thermal energy region are shown in Figure 1.1. In the figure it has been seen that, the data varies from 46 to 141 b at 0.0253 eV energy [13-17]. In these references, mixed neutron beams of thermal and epithermal energies were used for activation. They corrected the activity due to the epithermal neutrons by the Cd cut-off energy technique, which is complex and includes large uncertainty in the measured cross section [18-22]. For $^{55}Mn(n,\gamma)^{56}Mn$ reaction, the available literature data at thermal energy region are shown in Figure 1.2. In the figure it has been seen that, thermal neutron cross section data for $^{55}Mn(n,\gamma)^{56}Mn$ reaction, are also only available for 0.0253 eV and the reported data varies within 10.7 b to 13.64 b [23-29].

In the thermal energy region, evaluated neutron cross sections data are almost theoretically evaluated (except at 0.0253 eV). In this region, the cross section follows the well-known 1/v law of neutron capture, but the point of normalization is the value at 0.0253 eV. Therefore, if there is some discrepancy in that value, the values in the thermal region derived via the 1/v law

would also be not very reliable. It is therefore advisable to obtain experimental data at thermal energies other than 0.0253 eV to be able to check excitation function of a reaction at thermal energy region. Therefore, the thermal neutron capture (n, γ) cross section data at 0.0334 and 0.0536 eV are important to remove discrepancies on neutron capture cross sections as well as to validate evaluated nuclear data libraries at this energy region.

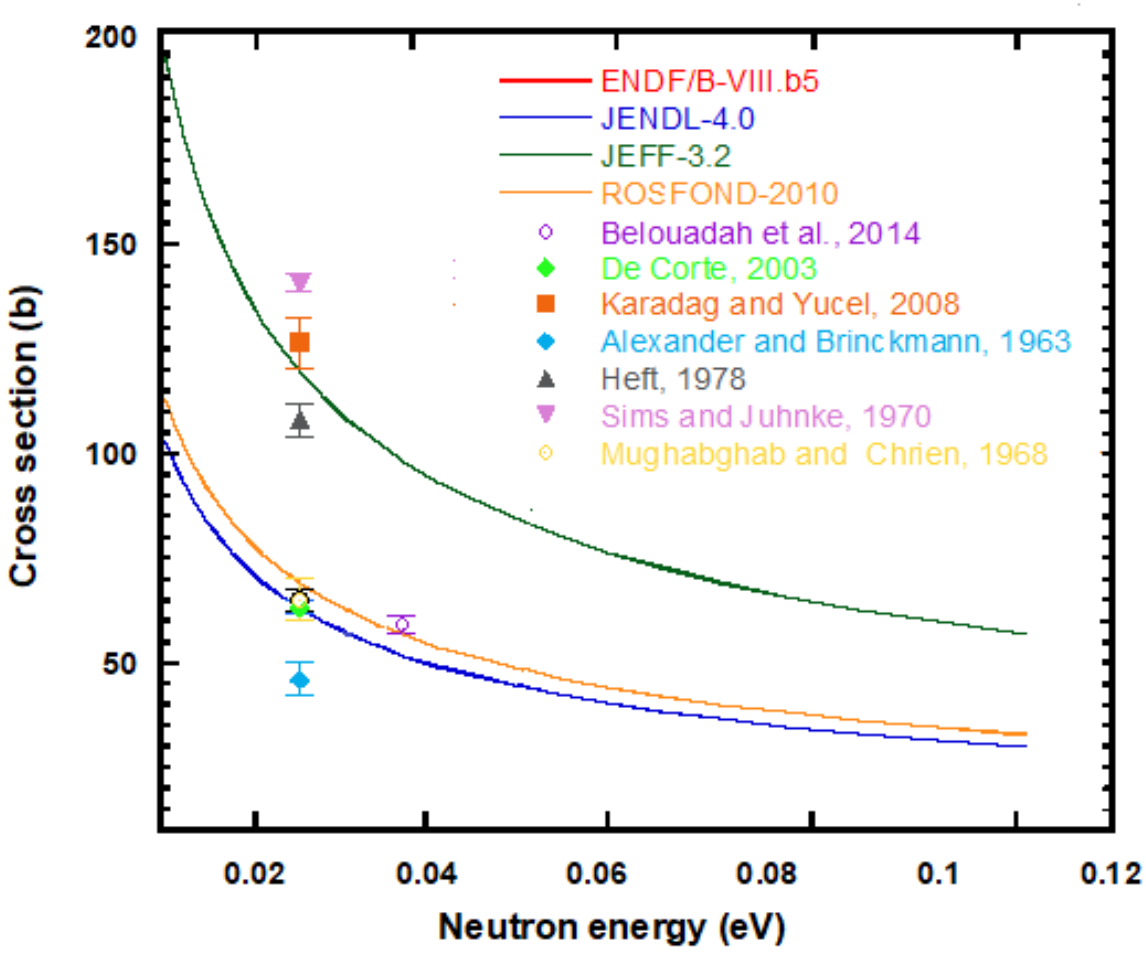

Figure 1.1: Cross sectional data available at thermal energy region for ^{174}Yb$(n,\gamma)^{175}$Yb reaction.

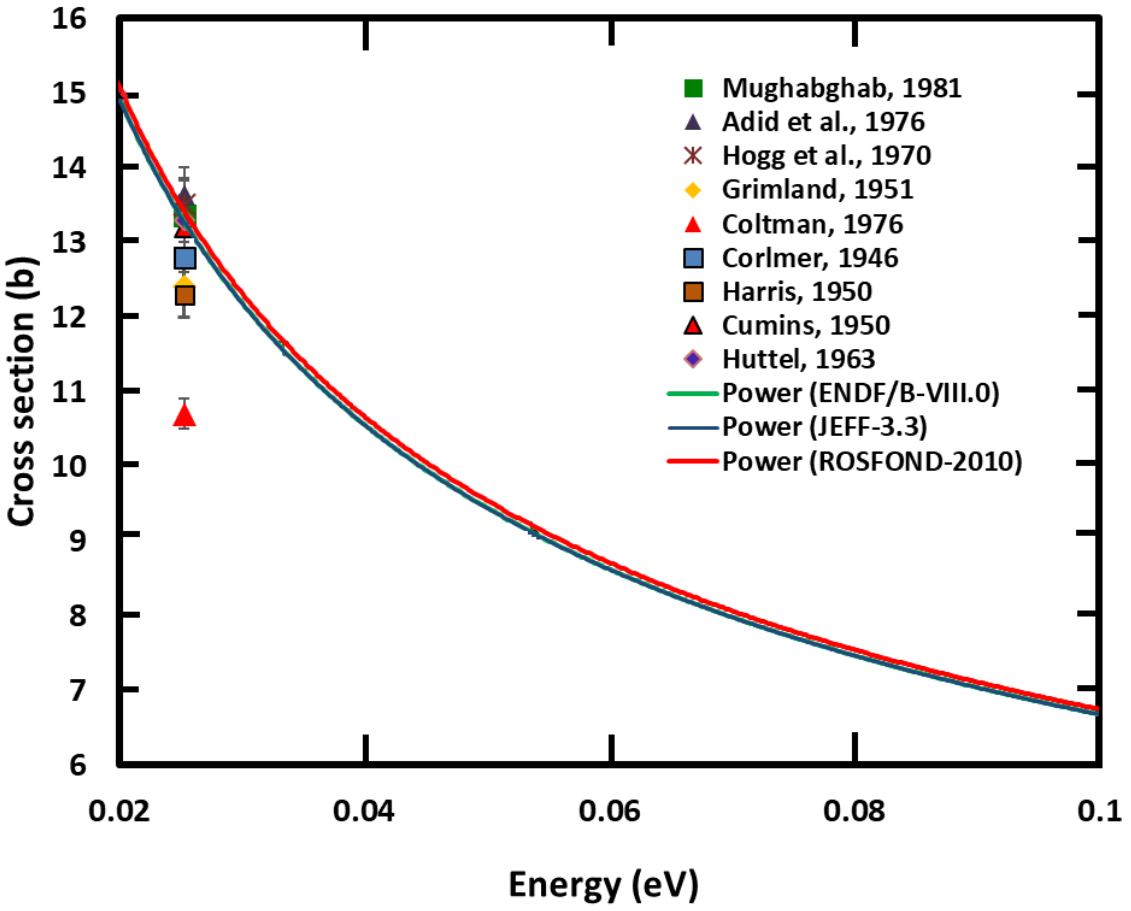

Figure 1.2: Cross sectional data available at thermal energy region for ^{55}Mn(n,γ)^{56}Mn reaction.

1.5 Objectives of This Study

The aim of this study is to determine the experimental neutron capture cross sections of ^{174}Yb$(n,\gamma)^{175}$Yb and ^{55}Mn$(n,\gamma)^{56}$Mn reactions at neutron energies of 0.0334 eV and 0.0536 eV. Therefore, the main objectives of this study are:

a. To measure cross-section of the reactions ^{174}Yb$(n,\gamma)^{175}$Yb and ^{55}Mn$(n,\gamma)^{56}$Mn by using monochromatic neutrons from TRIGA Nuclear Reactor at new energies of 0.0334 eV and 0.0536 eV.

b. To compare new excitation functions with the theoretically evaluated excitation functions of the nuclear data libraries like ENDF, JENDL etc.

c. To remove discrepancies of the available nuclear data of the mentioned reactions at average thermal neutron energy 0.0253 eV.

CHAPTER 2

LITERATURE REVIEW

A number of experiments have been done by the researchers to measure thermal neutron capture cross section of reactions $^{174}Yb(n,\gamma)^{175}Yb$ and $^{55}Mn(n,\gamma)^{56}Mn$. Most of the researchers measured neutron capture cross section at average thermal neutron energy 0.0253 eV and they used Cadmium cut off technique. The various experiments on $^{174}Yb(n,\gamma)^{175}Yb$ and $^{55}Mn(n,\gamma)^{56}Mn$ reactions at thermal energy region are discussed in this chapter.

1.1 Literature Survey on $^{174}Yb(n,\gamma)^{175}Yb$ Reaction

Mustafa Karadag and Haluk Yucel (2008) [5] measured the average thermal neutron capture cross section of reaction $^{174}Yb(n,\gamma)^{175}Yb$ is about 126.5±6.6 b. They used $^{55}Mn(n,\gamma)^{56}Mn$ monitor reaction to determine the neutron flux during the experiment. Analytical grade of MnO_2 and Yb_2O_3 powder samples with and without a cylindrical 1mm Cd shield box were irradiated in an isotropic neutron field obtained from three ^{241}Am-Be neutron sources each having 592 GBq activity installed at Ankara Nuclear Research and Training Center (ANRTC). They measured gamma-ray spectra for activated samples with a calibrated n-type high-purity Ge detector. Their experimental results were corrected for correction factors calculated for thermal and epithermal neutron shelf shielding effects, epithermal neutron spectrum shape and gamma ray self-attenuation .

Simonits et al. (1996) [7] recommended a cross sectional value of 62.5±0.75 b at average thermal neutron energy for the reaction $^{174}Yb(n,\gamma)^{175}Yb$. They used K_o-standardization method to re-evaluate cross section measurement based mainly on activation method. K_o method was intended to be an absolute technique where uncertain nuclear data are replaced by

compound nuclear constants K_o factors, which are experimentally determined with high accuracy.

De Corte (2003) [13] tabulated average thermal neutron absorption cross sections of 128 (n, γ) reactions of interest in NAA. He derived the values from the Y2K database of experimentally measured K_0-factors. He reported the average thermal neutron absorption cross section of $^{174}Yb(n,\gamma)^{175}Yb$ reaction is 63.4± 1.7 b in his compilation.

The thermal neutron capture cross section of the reaction $^{174}Yb(n,\gamma)^{175}Yb$ at 0.0372 eV measured by the N. Belouadah et. al. (2013) [19] is 59.07 ± 2.3 b. They used $^{197}Au(n,\gamma)^{198}Au$ monitor reaction to determine the neutron flux during the experiment. The irradiation performed at horizontal channel of Es-Salam Nuclear Research Reactor of Algeria. High purity Germanium (HPGe) detector was used to determine the activity of product nuclides. Correction factors such as neutron self-shielding and gamma ray attenuation effects were considered. They extrapolated their experimental result at 0.0253 eV and it is 71.6 ± 2.7 b.

G. H. E. Sims and D. G. Junhnke [20] measured average thermal neutron capture cross section of $^{174}Yb(n,\gamma)^{175}Yb$ reaction is 141± 2 b. They used Cadmium cut off technique. The ^{174}Yb target solutions as chlorides in dilute HCl were pipetted into flat aluminium pellets, which were then sealed. The samples were placed in aluminium irradiation cans together with cobalt tags and blanks. They carried out their samples irradiation in pairs, with one set of samples surrounded by a 0.040 inch thick cadmium shield. They irradiated their samples by using a well-thermalized position just outside the calandria of the NRX reactor at Chalk River Nuclear Laboratories. They measured the activity of the samples by using 2in.×2in. NaI(TI) Scintillation detector. Their measurements are relative to a ^{59}Co cross section of 37.5 b.

Heft (1978) [21] measured average thermal neutron cross section of ^{174}Yb$(n,\gamma)^{175}$Yb reaction is 108± 4 b by Cd cut off technique. He used element Sc-46 as an internal flux monitor. Irradiation of samples were carried out at the Lawrence Livermore Laboratory LPTR research reactor facility. He used gamma spectral analyzer to measure absolute photon emission rates.

1.2 Literature Survey on ^{55}Mn$(n,\gamma)^{56}$Mn Reaction

Coltman and Goldhaber (1946) [22] measured the manganese corss section to be 10.7±0.2 b based on a boron value of 600 b. There is no discussion of self-shielding or foil size. They only considered the errors due to statistical counting and scattering cross section to calculate the scattering correction.

Adib et al. (1976) [23] measured the total cross section of manganese and obtained a 1/v component corresponding to a cross section of 13.64± 0.19 b. No discussion about error analysis is found in their literature.

Grimeland et al. (1956) [24] measured the pile oscillator cross section of manganese to be 12.4± 0.2 b relative to boron value of 710 b.

Huttel and Liewers (1963) [25] measured the Mn absorption cross section in a pile oscillator in the Ressendrof reactor. A value of 13.3± 0.03 b is obtained relative to boron value of 755 b.

Cumins (1950) [26] measured the Mn absorption cross section is 13.2± 0.2 b relative to a boron value of 783 b.

Colmer and Littler (1946) [27] measured the pile oscillator absorption cross section of Mn is 10.7± 0.2 b relative to a boron value of 710 b. They note that, no chemical analysis was performed, a large systemic error is possible and an unspecified shelf-shielding correction was applied.

Harris et al. (1950) [28] measured the manganese cross section is 12.3 b in a pile oscillator relative to a natural boron value of 710 b. Correction for resonance absorption cannot be made since solid manganese of unspecified diameter was irradiated.

Hogg et al. (1970) [29] measured the cross section of manganese 13.5±0.5 b relative to a cobalt cross section 37 b. Cadmium-covered activity was used to correct the measured total activity . No information is found about cadmium ratios, self-shielding, size of the detectors and energy or intensity of gamma radiation studied.

CHAPTER 3

METHODOLOGY

This chapter covers a brief description about Neutron Activation Analysis method that we used to measure neutron absorption cross section, TRIGA Mark-II Research Reactor where the sample targets were irradiated and Gamma Ray Spectroscopy.

3.1 Neutron Activation Analysis

Neutron Activation Analysis (NAA) is a sensitive nuclear analytical technique where radiative neutron capture reaction is prominently applied to determine elemental content in an unknown sample and can also be applied for nuclear data measurements. According to the IAEA,

"Neutron activation analysis is a method for the qualitative and quantitative determination of elements based on the measurement of characteristic radiation from radionuclides formed by irradiating materials by neutrons".

Neutron activation analysis (NAA) was discovered in 1936 when Hevesy and Levi found that samples containing certain rare earth elements became highly radioactive after exposure to a source of neutrons. From this observation, they quickly recognized the potential of employing nuclear reactions on samples followed by measurement of the induced radioactivity to facilitate both qualitative and quantitative identification of the elements present in the samples.

3.2. Principle of Neutron Activation Analysis

The principle involves in NAA consists of first irradiating a sample with neutrons from a neutron source such as research reactor, accelerator etc. to produce specific radionuclides. As

the sequence of events occurring during the most common type of nuclear reaction used for NAA, namely the neutron capture or (n,γ) reaction is illustrated in Figure 3.1.

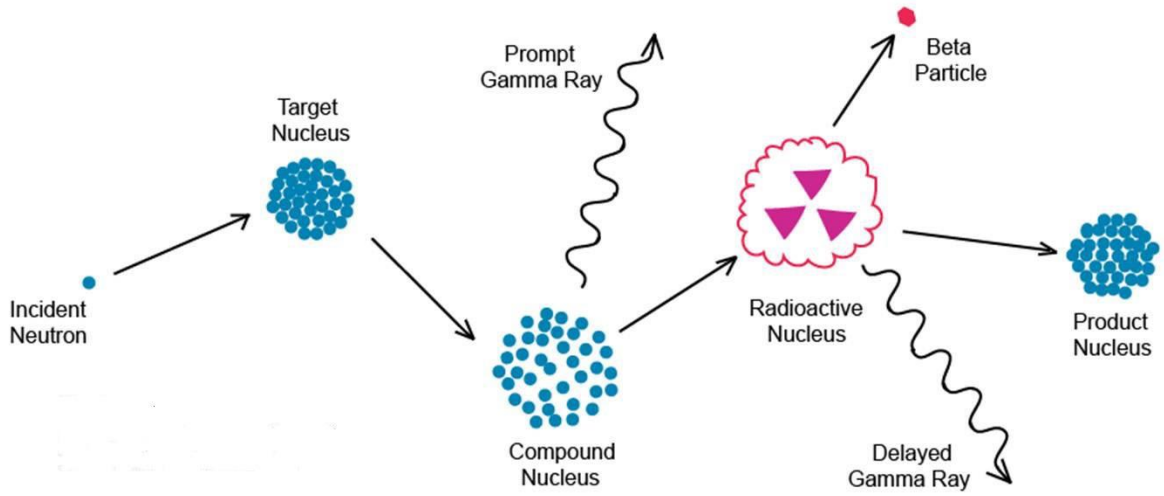

Figure 3.1: Interaction of incident neutron with target nucleus.

When a neutron interacts with a target nucleus via an inelastic collision a compound nucleus forms in an excited state. The excitation energy of the compound nucleus is gained due to the addition of binding energy of the neutron with the nucleus. The compound nucleus will almost instantaneously de-excite into a more stable configuration through emission of one or more characteristic prompt gamma rays. In many cases, this new configuration yields a radioactive nucleus which also de-excites (or decays) by emission of one or more characteristic delayed gamma rays, but at a much slower rate according to the unique half-life of the radioactive nucleus. Depending upon the particular radioactive species, half-lives can range from fractions of a second to several years.

3.3. Theory of Neutron Activation Analysis

When neutron interacts with a target nucleus, a compound nucleus is formed. The compound nucleus has a certain finite life time (10^{-13} to 10^{-15} s) during which it remains highly excited state due to high binding energy and kinetic energy of the incident neutron in the nucleus. De-excitation of the compound nucleus can occur in different ways that are independent of the way the compound nucleus is formed. Each of this process has a certain probability, depending on the nuclear cross section of the each mode, which is related to the excitation of the compound nucleus.

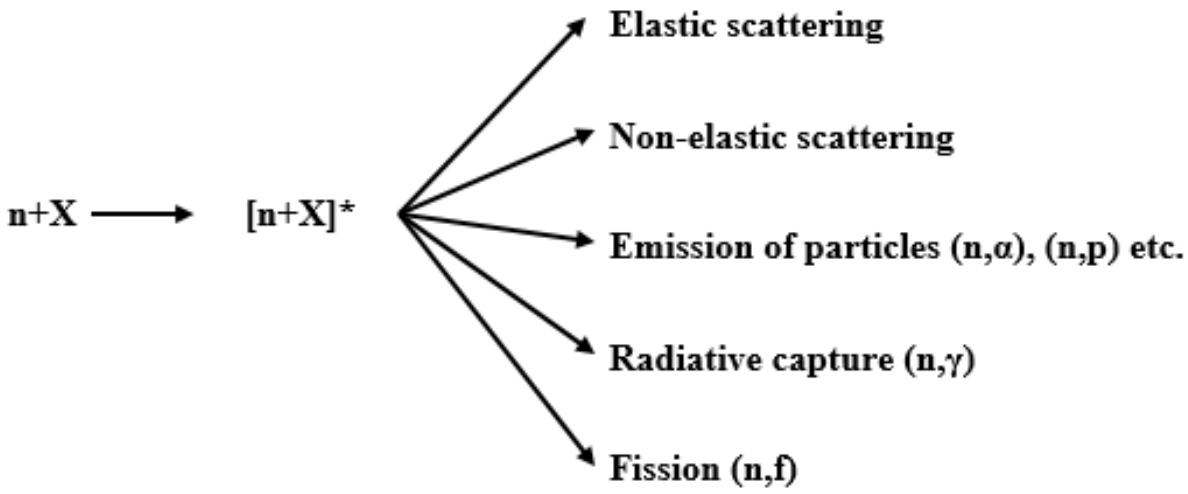

Figure 3.2: Probability of occurring nuclear reaction.

3.4 Classification of Neutron Activation Analysis

Neutron activation analysis should be classified as follows:

a) Instrumental neutron activation analysis (INAA)

b) Radiochemical neutron activation analysis (RNAA)

c) Prompt gamma ray neutron activation analysis (PGNAA)

d) Delayed gamma ray neutron activation analysis (DGNAA)

e) Epithermal neutron activation analysis (ENAA)

f) Fast neutron activation analysis (FNAA)

3.4.1 Instrumental neutron activation analysis (INAA)

NAA with the use of automate sample handling, gamma ray measurement with solid state detectors and computerized data processing is generally possible to simultaneously measure more than thirty elements in most sample types without chemical processing. The application of purely instrumental procedures is commonly called the instrumental neutron activation analysis and is one of NAA's most important advantages over other analytical techniques. INAA is often referred to as nondestructive NAA.

3.4.2 Radiochemical neutron activation analysis (RNAA)

NAA in which chemical separations are done to samples after irradiation to remove interferences to concentrate the radioisotope of interest, the technique is called radiochemical neutron activation analysis (RNAA). The technique referred as destructive NAA and is performed infrequently due to its high labor cost.

3.4.3 Prompt gamma ray neutron activation analysis (PGNAA)

The PGNAA technique is generally performed by using a beam of neutrons extracted through a reactor beam port. Fluxes on samples irradiated in beams are on the order of one millions times lower than on samples inside a reactor but detectors can be placed very close to the sample compensating for much of the loss in sensitivity due to flux. The PGNAA technique is most commonly used for determination of lighter elements (H, B, Si etc.) and elements with extremely high neutron capture cross section (B, Cd, Sm and Gd); elements which decay too rapidly to be measured by delayed gamma ray neutron activation analysis (DGNAA).

3.4.4 Delayed gamma ray neutron activation analysis (DGNAA)

DGNAA is useful for the vast majority of elements that produce radioactive nuclides. The technique is flexible with respect to time such that the sensitivity for long lived radionuclide that suffers from interference by a shorter lived radionuclide can be improved by waiting for the short-lived radionuclide to decay. The selectivity is a key advantage of DGNAA over other analytical methods.

3.4.5 Epithermal neutron activation analysis (ENAA)

ENAA is useful when the nuclides of interest have much higher nuclear cross section (n,ɣ) by resonance capture of epithermal neutrons than the thermal neutrons, while the interfacing elements have not or have lower reaction cross sections, the activity by epithermal neutrons can considerably increase the sensitivity of the detection for an element.

3.4.6 Fast neutron activation analysis (FNAA)

When the measurements of the elements (lighter elements such as C, N, O, F and S) by thermal neutron is not favorable because of the very low (n, ɣ) cross section, the first neutron (14 MeV)

can be used to produce reaction of (n, 2n), (n.α), (n,p) and (n,n). The advantages of 14 MeV NAA are that it is fast and nondestructive, can be used on a routine basis, is ideal for short irradiations and is particularly sensitive for detection of lighter element.

3.5 Fundamental Equation for INAA Method

INAA can be treated mathematically such as in two ways:

a) Absolute INAA method

b) Comparative INAA method

3.5.1 Absolute INAA method

When a sample is irradiated by a constant neutron flux, then the rate of formation of a radionuclide in neutron activation is expressed as

$$\frac{dN^*}{dt} = \sigma \Phi N \tag{3.1}$$

Where, N^* is the number of activated nuclei at time t, σ is the cross-section, in barn, Φ is the neutron flux density and N is the number of the target nuclei.

If the nuclide formed is radioactive, it will decay with time, the decay rate of the radionuclide being

$$\frac{dN^*}{dt} = -\lambda N^* \tag{3.2}$$

Here, $\lambda = {ln2}/{T_{2/1}}$ is the decay constant of the activated nuclide and $T_{2/1}$ is the half-life of the activated nuclide. Therefore, the production rate of the activated nuclide is expressed as

$$\frac{dN^*}{dt} = \sigma \Phi N - \lambda N^* \tag{3.3}$$

After solving equation (3.3), the activity or disintegration rate (A) at the end of irradiation time t_i is then

$$A = \sigma\Phi\frac{MN_A\theta}{W}\{1 - e^{-\lambda t_i}\} \tag{3.4}$$

$$\sigma = \frac{AW}{\Phi MN_A\theta} \times \frac{1}{\{1-e^{-\lambda t_i}\}} \tag{3.5}$$

Where,

M is the mass of the element

$N_A = 6.023\times10^{23}$, is the Avogadro's number

θ is the isotopic abundance

W is the atomic weight

Usually, in neutron activation analysis, the activity of the radionuclide is measured experimentally in a sample to deduce the unknown mass (M) of the element by the above equation.

Correction must be made in activity of the product nuclide for the decay period t_d and counting period t_c, where,

Decay factor, $F_d = e^{-\lambda t_d}$ and

Counting factor, $F_c = \frac{1-e^{-\lambda t_c}}{\lambda t_c}$

So, the basic equation for INAA in absolute method becomes,

$$A = \frac{MN_A\theta}{W}\sigma\Phi F\left\{1 - e^{-\lambda t_i}\right\}\left\{e^{-\lambda t_d}\right\}\left\{\frac{1-e^{-\lambda t_c}}{\lambda t_c}\right\} \tag{3.6}$$

Hence,

$$\sigma = \frac{AW}{N_A\Phi M\theta\{1-e^{-\lambda t_i}\}\times F_d\times F_c} \tag{3.7}$$

All the factors on the right of the above equation are in principle, known or can be measured. Thus, it can be possible to calculate the neutron absorption cross section of the experimental target for a certain neutron energy.

The difficulty of measurement of σ accurately leads to the difficulty of measuring neutron flux density Φ and also the value of Φ changes depending on time and the location in most powerful neutron sources like nuclear reactors, sample and its container cause perturbation of neutron flux density (flux depletion and self-shielding of neutrons), which is very difficult to evaluate precisely.

The activity A can be obtained from the following relationship,

$$A = R/ I_\gamma \varepsilon \tag{3.8}$$

Where, R is the counting rate of full energy peak caused by the gamma rays used for the activity measurement, ε is the absolute counting efficiency of the gamma ray detector, and I_γ is the intensity of gamma rays.

3.5.2 Comparative INAA method

In the comparative INAA method, an element "X" in a sample and a known amount of the same element "X" as a standard are irradiated together and both sample and standard are counted under exactly the same conditions by the radiation detector. This procedure eliminates any uncertainty in the parameter σ, ϕ, λ and in the decay scheme and detection efficiency. The NAA equation by the comparative method is thus reduced to a simple form, as shown below

$$\frac{Mass\ of\ element\ \text{"X"}\ in\ sample}{Mass\ of\ element\ \text{"X"}\ in\ standard} = \frac{A_x\ in\ the\ sample \times (e^{\lambda t_d})sam}{A_x\ in\ standard \times (e^{\lambda t_d})std} \tag{3.9}$$

Knowing the activities of X in sample and standard, the sample and standard decay times and the mass of the element “X” in the standard, the mass of the element “X’’ is then calculated.

3.6 Advantages of NAA Technique

The advantages of NAA technique are given below:

- Non-destructive and multi-elemental technique
- Almost negligible matrix effects
- Minimal sample preparation for solid samples
- Fewer errors during sample preparation by contamination and loss of elements
- Organic material from biological samples in solids can be tolerated without elimination by ashing
- High potential sensitivity
- Good precision and accuracy also at the trace level

3.7 Limitations of NAA Technique

The NAA technique has the following limitations:

- Need for an expensive neutron source like nuclear research reactor and radioactive control room laboratory
- Often a long analysis time for activation and cooling
- Interference by other activation products or fission products of uranium.

3.8 TRIGA Mark II Research Reactor

The TRIGA Mark-II research reactor of Bangladesh Atomic Energy commission is a light water cooled, graphite reflected reactor, designed for steady state and square wave power level of 3 MW (thermal) and for pulsing with maximum power level of 852 MW. The characteristics of this reactor is clear from the name "TRIGA" which a combination of words Training, Research, Isotope production and the name of manufacturing company General Atomic Company, USA. The installation of the reactor started at the end of 1980 and reactor achieved its first criticality at 50 W in September 1986 and was commissioned to steady state power of 3 MW in October 1986. The reactor is used for various field of nuclear research like neutron activation analysis, neutron radiography, neutron scattering, radioisotopes production etc. A brief description about components of TRIGA Mark-II reactor are discussed below.

Figure 3.3: TRIGA MARK-II Research Reactor (3 MW).

3.8.1 Reactor tank

The reactor tank is made of aluminum alloy of type 6061-T6 which is installed inside the reactor shield structure. The length and diameter of the tank is 8.23 m and 1.98 m, respectively. The tank is filled up with 24,865 liters of demineralized water. The reactor core is located near the bottom of the reactor tank.

3.8.2 Reactor core

Nuclear reactor consist of an active part in which fission chain reaction are sustained and most of the fission energy is released as heat. This active part is known as core, which contain nuclear fuel rod and moderator. The reactor core consists of 100 fuel elements (including 5 fuel follower control rods and 2 instrumented fuel elements), 1 air follower control rod, 18 graphite dummy elements, 1 DCT, 1 pneumatic transfer system irradiation terminus (Rabbit system) and 1 Am-Be neutron source (strength: 3 Ci).

3.8.3 Control rod

The neutron flux in the reactor has been controlled by six control rods, which contain boron carbide (B_4C) as the neutron absorber material. When those rods are fully inserted into the reactor core, the rods absorb the neutrons continuously emitted from the start-up sources (3 Ci of Am-Be source) and the reactor remains sub-critical. If the absorber rods are withdrawn from the core, the number of fission in the core and the power level increase. The reactor start up process takes roughly 10 minutes to reach a level of 3 MW from the sub-critical state. Control rods are mainly classified as shim, regulating and safety rods. Shim rods are used for coarse control of reactor power, regulating rod are used for fine control and the safety rods are used for scram on shut down of the reactor. Each control rod is a sealed aluminum tube containing powder of boron carbide as neutron a poison. Each control rod are approximately 51cm long.

3.8.4 Reflector

The reflector of TRIGA reactors is a ring shaped block of graphite that surrounds the core radially. The graphite is protected from water by a leak-tight welded aluminum can. The purpose of reflector is to decrease the loss of neutrons from the core by reflecting back some of neutrons which tends to leak out or escape.

3.8.5 Coolants

The heat generated in the reactor core is removed and dissipated to the atmosphere by a cooling system consisting of primary and secondary cooling system. The circulation of suitable coolant removes the heat generated in the core. Some of commonly used coolants are light water, heavy water, liquid sodium or potassium, certain organic compounds air, carbon di oxide and helium. In the TRIGA Mar-II reactor, demineralized light water is used as coolant.

3.8.6 Reactor shielding

In nuclear reactor a provision is always made for attenuating the nuclear reactions that escape from the system by placing some barriers capable of absorbing them. Mainly such barrier is known as shielding. Shielding are necessary for the protection for the personal as well as capable for the protection of reactor control equipment from high radiation background. The reactor shield or TRIGA Mark-II research reactor is made of heavy reinforced concrete structure, standing 7.9 m above the reactor hall.

3.9 Irradiation Facilities of TRIGA Mark-II Research Reactor

The following irradiation facilities of TRIGA Mark-II reactor have been established to provide intense neutrons fluxes for research and isotope production.

1. Rotary specimen rack (Lazy Susan)
2. Pneumatic transfer system (Rabbit)
3. Dry Central thimble
4. Beam port facilities

3.9.1 Rotary specimen rack (Lazy Susan)

The rotary specimen rack/Lazy Susan is a donut shaped watertight device placed in the upper part of the graphite reflector assembly around the reactor core. This rack facilitates 41 sample-holding tubes. Each of these tubes (except the 1st one) can accommodate two standard specimen containers. The dimension of the each specimen container is 13.9 cm long and 3.18 cm dia. Sample is loaded into the rotary specimen rack through the 3.3 cm dia loading tube, which extends up to the top of the reactor shield structure and terminate at the center channel. A position control mechanism allows loading of samples in different chambers of the Lazy Susan. This facility is used for neutron activation analysis as well as isotope production. The neutron flux in this facility is 1.23×10^{13} n/cm^2/sec.

3.9.2 Pneumatic transfer system (PTS)

The PTS is also called the Rabbit System. It is used for the production of very-short-lived radioisotopes. It transfers the sample to be irradiated into the reactor core or out from the reactor core in about 4.6 sec. The neutron flux in this facility is 1.91×10^{13} n/cm^2/sec.

3.9.3 Dry central thimble

In the DCT, samples may be exposed to a maximum neutron flux density of 9.12×10^{13} n/cm^2/sec. The DCT is used for radioisotope production and various R&D purposes.

3.9.4 Beam port facilities

There are four neutron beam ports, named as

1. Tangential beam port,
2. Piercing beam port,
3. Radial beam port #1
4. Radial beam port #2.

The four beam ports are shown in Figure 3.4.

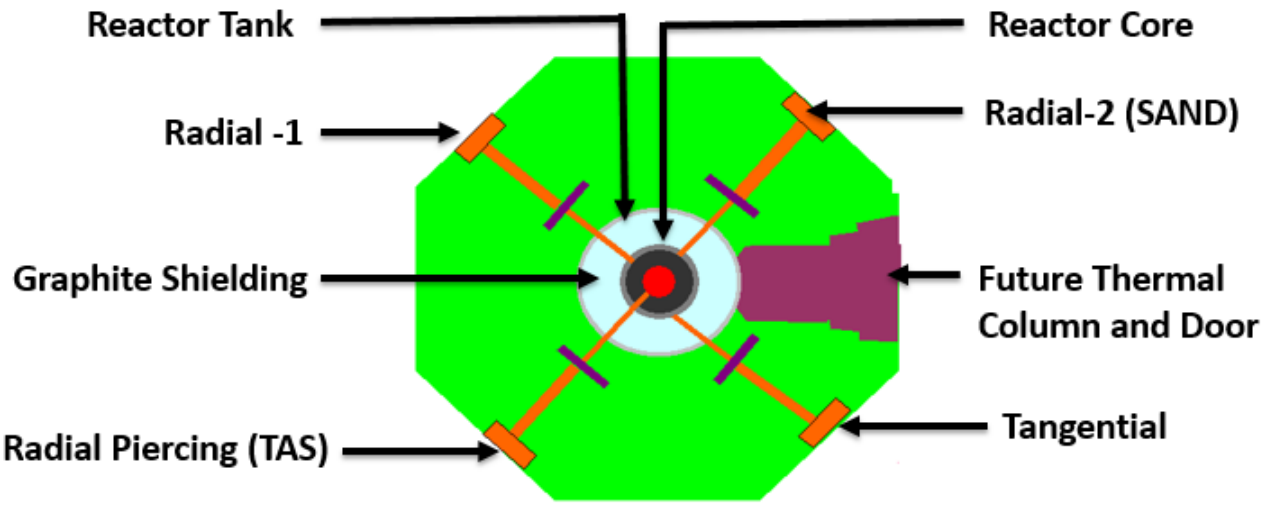

Figure 3.4: Beam ports of TRIGA Mark-II.

The tangential beam port is used for neutron radiography. The neutron flux in the tangential beam port at a distance of 140 cm from the wall to the sample is 1.13×10^{6} n/cm^2/sec. The piercing beam port is being used for neutron scattering studies by using Triple Axes Spectrometer (TAS). Radial beam port #2 is being used for SAND and another radial beam port is unused.

Since our targets were irradiated at Triple axis spectrometer (TAS) and Savar neutron diffractometer (SAND), so the two facilities are discussed here:

Triple axis spectrometer (TAS)

Neutrons from core of the reactor pass through a shielded collimator to the Cu(200) monochromator at radial piercing beam port. Bragg reflection is used to do monochromatization of the neutrons very effectively from mosaic Cu(200) single crystal. The plane of Cu(200) single crystal ($5 \times 15 \times 1.2$ cm^3) was inclined in a position such that neutron beam of single wave length $\lambda = 1.2360$ Å, corresponds to 0.0536 eV was obtained. Before hit the sample target, the monochromatic neutrons reflect through a Soller collimator of internal area 5×5 cm^2 and then pass through another collimator of internal area 1.6×5.0 cm2. The last collimator ($50 \times 50 \times 20$ cm3) made of polybron also act as shielding to minimize neutron background level at the sample position. Schematic diagram of experimental setup in TAS shown in Figure 3.5.

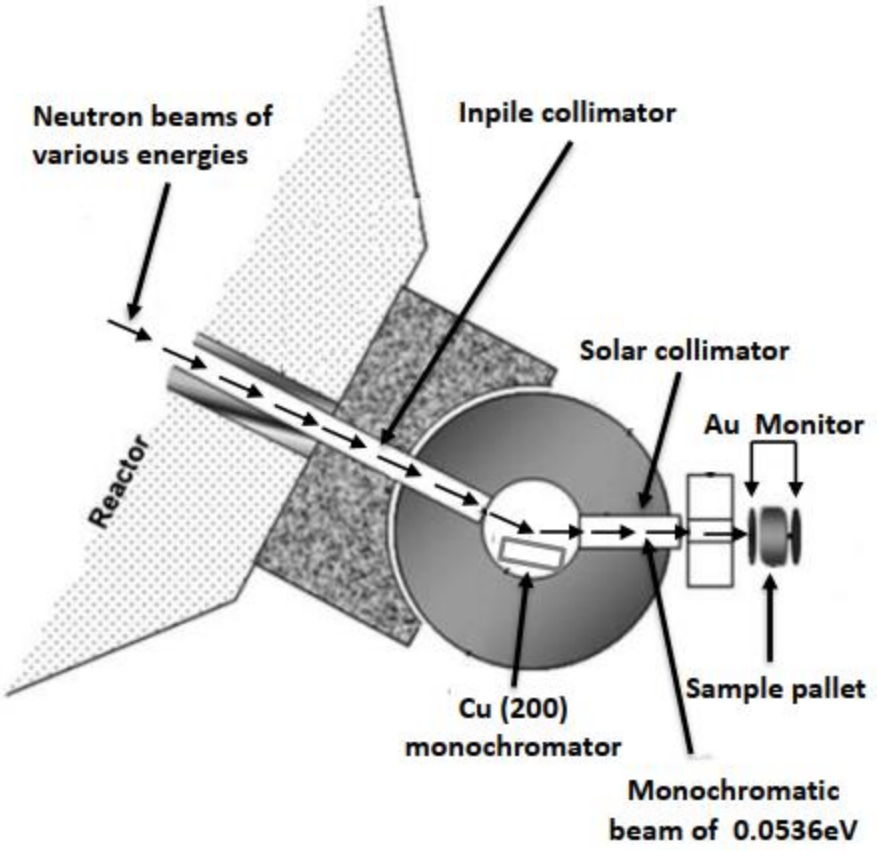

Figure 3.5: Schematic diagram of experimental setup in TAS.

Savar neutron diffractometer (SAND)

Neutrons of different wave length from the reactor core through radial beam port-2 were moved across a sapphire crystal of 12.7 cm in diameter and 12.24 cm in length, fixed in the tapered section at the (upstream) end of the collimator to filter the neutrons before entering the monochromator. Nine single crystal silicon labs of dimension 1.45 × 0.53 × 19.05 cm^3, cut from the silicon wafer of same 0.6 cm thickness were used to fabricate the monochromator. Blocks of internally heavy reinforced concrete with dimension of 228 × 172 × 176 cm^3 is used to shield the monochromator. The neutrons of certain wavelength can be separated efficiently by using Bragg reflection from a single crystal of Si(115). For the purpose of proper reflection

of Si(115), the monochromator is positioned at the top of bending screw. The thickness, offset angle and bending radius of silicon slabs have been selected to optimize the intensity and diffractometer resolution for the Si(115) reflection at 97^0 take-off angle and yielding a wave length of $\lambda = 1.5656$ A° corresponds to 0.0334 eV energy. Schematic diagram of experimental setup in SAND shown in Figure 3.6.

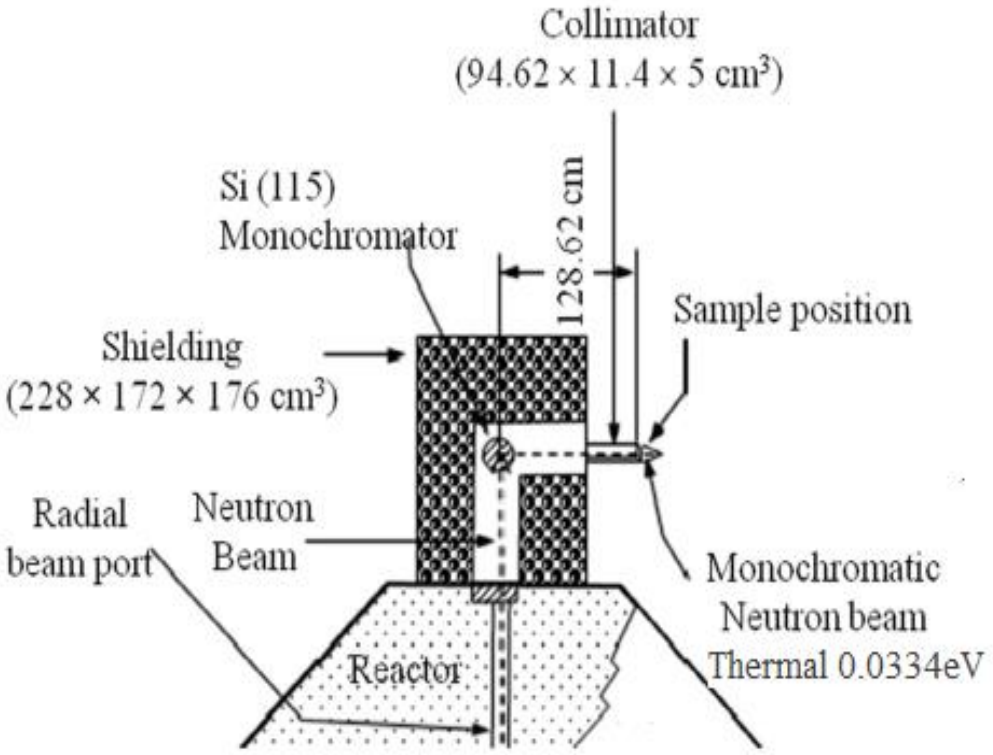

Figure 3.6: Schematic diagram of experimental setup at SAND.

3.10 Gamma Ray Spectroscopy

Gamma spectroscopy is a radio analytical measurement technique, the best for identification and quantification of radionuclides using germanium detectors, while a Geiger counter determines only the count rate, a gamma spectrometer will determine the energy and the count rate of gamma rays emitted by radioactive substances. This is due to the characteristic discrete energies of gamma rays produced by radioisotopes, which is the basics of gamma spectroscopy (Gammas and X-rays are usually properties of the daughter nucleus). By measuring the energies of gamma ray photons, the source of radiation can be determined by comparison of the observed photo peaks to a library of known gamma emitting source energies. The net count in the photo peak area is related to element activity or concentration of the radioisotope. The method is thus a powerful tool for monitoring the radiation environment. The combination of absorption coefficient, semiconductor properties and availability in a suitably pure state makes germanium the predominant material for high.

3.11 General Consideration in Gamma-Ray Spectroscopy

An X-ray or gamma ray photon is uncharged and creates no direct ionization or excitation of the material through which it passes contrary to charged particles (e.g. alpha and beta). The detection of gamma rays is therefore critically dependent on causing the gamma-ray photon to undergo an interaction that transfers all or part of the photon energy to charged particles in the absorbing material which can be collected together to produce an electrical signal. The detection of gamma rays depends on interactions as photoelectric effect, Compton scattering and pair production, which transfer gamma ray energy to electrons within the detector material. The excited electrons then lose energy by ionization. These charged pairs produced by the

primary electrons are electron-hole pairs whose number corresponds to the energy of primary electrons. The detector must be constructed of suitable material so that the electron hole pairs can be collected and presented as electrical signal.

The properties that should be considered for an ideal detector for gamma spectroscopy are:

- Output proportional to gamma-ray energy.
- Good efficiency, i.e. high absorption coefficient
- Easy mechanism for collecting the detector signal
- Good stability over time, temperature and operating parameters
- Reasonable cost
- Reasonable size

3.12 Gamma-Ray Spectroscopy with Semiconductor Detector

For a detector serving as a gamma-ray spectrometer, it must carry out two distinct functions; i.e. first it must act as a conversion medium with reasonable probability of gamma ray interaction yielding one or more fast primary electrons; second, it must function as a conventional detector for secondary electrons. The requirement of full absorption of the secondary electron rules out gas-filled detectors for the spectroscopy of gamma rays, other than those with very low energy.

The penetration distance of a 1 MeV electron in standard temperature and pressure (STP) gases is several meters, so that detectors of any practical size can never come close to absorbing all the secondary electron energy. For the measurement of gamma rays above several hundred keV, there are two detector categories of major importance, inorganic scintillators as NaI(Tl) and semiconductor detectors. The scintillators have the advantage of availability in large size

and high density, which can result in high interaction probabilities for gamma rays. Due to the high atomic number of iodine, a large number of all interactions will result in complete absorption of gamma-ray energy, so the photo fraction will be high. The energy resolution of

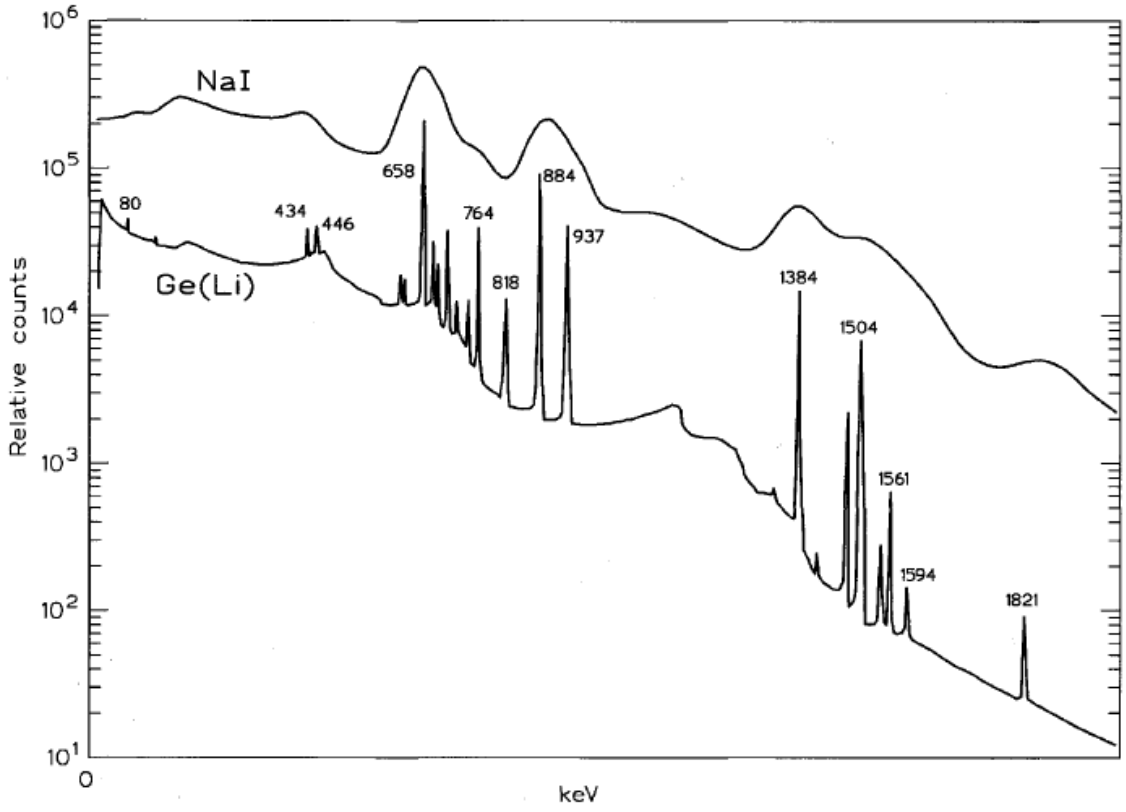

Figure 3.7: Comparative pulse height spectra recorded using a sodium iodide scintillator and a Ge(Li) detector. The source was gamma radiation from the decay of ^{108m}Ag and ^{l10m}Ag. Energies of peaks are labeled in keV [30].

scintillators is poor. Figure 3.7 shows comparative spectra with germanium and shows that it is better choice for separation of closely spaced gamma energies. The typical energy resolution of a good germanium system is few tenths of a percent compared to 5-10 % for sodium iodide. The smaller size available and the lower atomic number of germanium contribute to give photo peak efficiencies an order of magnitude lower in typical cases. Moreover, the photo fractions are low and thus the quanta in the pulse height spectra are more of a problem. On the other

hand, the good resolution of the semiconductor detectors aids in the detection of weak sources of discrete energies when superimposed on a broad continuum.

3.13 High Purity Germanium Detector

The semiconductor materials are good for the electron-hole pair collection within the detector; this must be done within a reasonably short time. Moreover, there must be no traps, which can prevent them reaching the collecting contacts. Trapping centers can be due to

- Impurities within the semiconductor lattice
- Interstitial atoms and vacancies within the lattice due to structural defects
- Interstitial atoms caused by radiation damage

This implies that the detector material should be of high purity and nearly perfect crystalline state. Germanium is the most commonly used detector material for its higher atomic number (as compared to Silicon) which makes it practicable for detection of higher energy gamma radiation. Over recent years, the technology for the manufacture of high purity germanium with a suitable degree of crystal perfection is achieved. When an n+ layer is created on a face of a high-purity p-type germanium slab and a reverse bias is applied to the detector, a depletion layer throughout the p-type material is formed. Such a detector is called hyper-pure or simply high-purity germanium detector abbreviated as HPGe.

3.14 Packing of the Detector

HPGe detectors are maintained within an evacuated metal container (usually aluminum) referred to as the can. The detector crystal inside the can is in thermal contact with a metal rod called a cold finger. The combination of metal container and cold finger is called the cryostat. The cold finger extends past the vacuum boundary of the cryostat into a Dewar flask that is filled with liquid nitrogen. The immersion of the cold finger into the liquid nitrogen maintains the HPGe crystal at a constant low temperature. This helps to ensure the reproducibility of the electronic measurement (reduce electronic noise) and thereby achieve as a high resolution as possible. The construction of the cryostat must take into account a number of factors;

- The detector should be maintained at a temperature close to 77 K
- The detector cap must be thin enough to allow the gamma-radiation to penetrate but still withstand the vacuum and provide a reasonable degree of protection to the detector
- The cryostat construction must isolate the detector from mechanical vibration
- The cryostat's material should be specially selected if the detection system is set for low background measurements

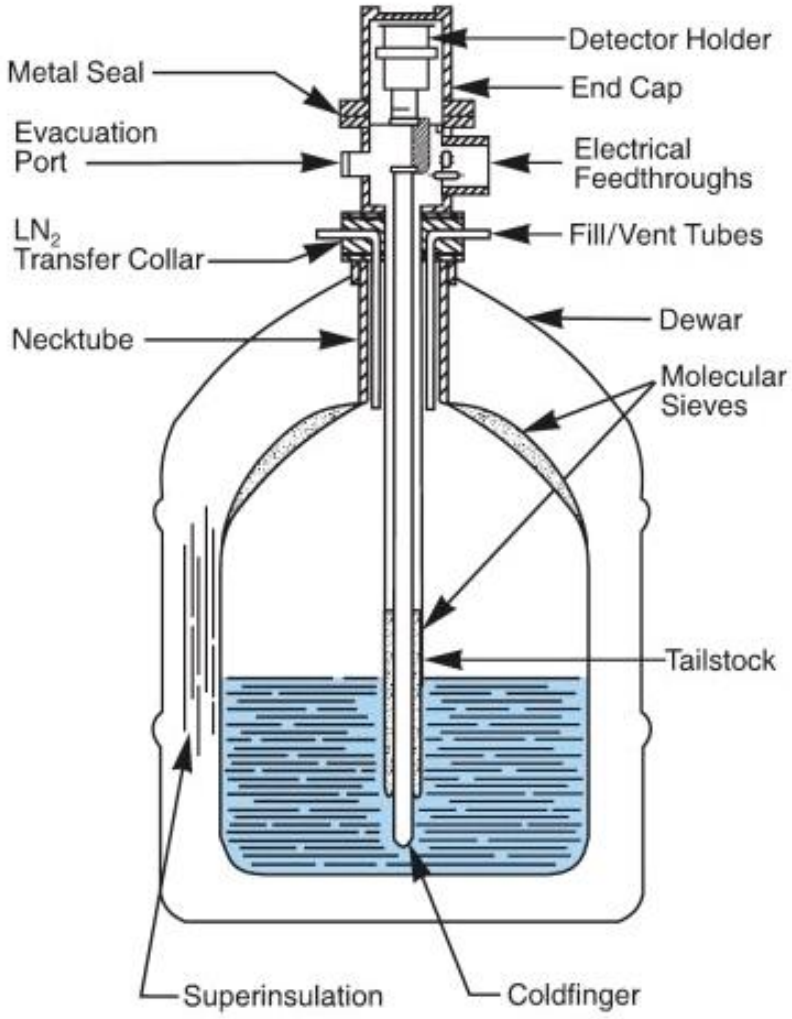

Figure 3.8: A typical germanium detector, cryostat and liquid nitrogen reservoir.

3.15 Electronics for Gamma-Ray Spectrometry

The output from a gamma-ray detector is an amount of electrical charge proportional to the amount of gamma-ray energy absorbed by the detector. The function of the electronic system is to collect that charge, measure the amount and store the information. A typical simple electronic system for gamma-ray spectroscopy is shown in Figure-3.9.

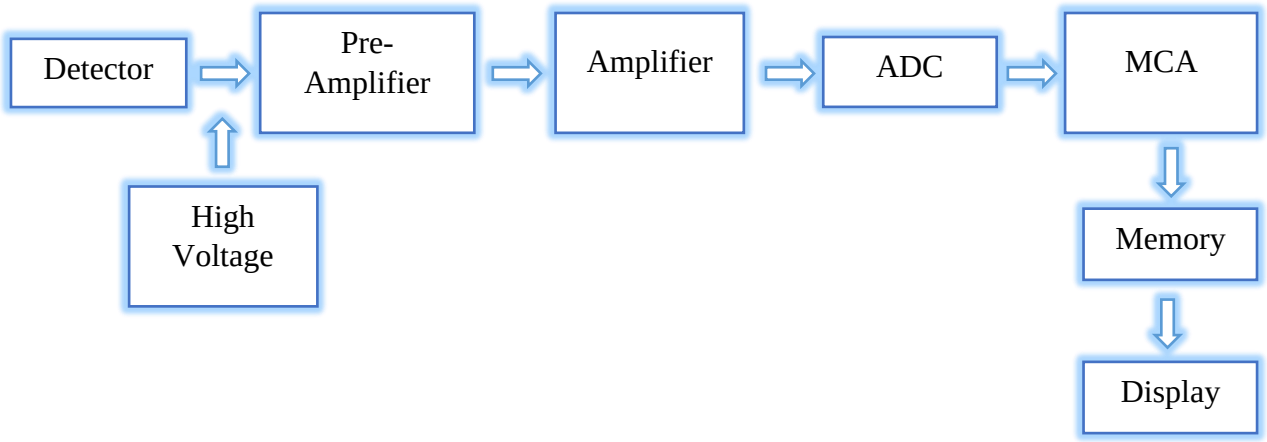

Figure 3.9: A simple schematic diagram of a gamma spectroscopy system.

The gamma photons produce electron-hole pairs and the electrons and holes are collected by an applied electrical field supplied by the bias supply. The charge sensitive pre-amplifier detects the charge produced in the crystal, and produces an electrical pulse suitable for direct amplification. The linear amplifier changes the pulse shape and increases it size. The multichannel analyzer (MCA) sorts the pulses by the pulse height and counts the number of pulses within individual pulse height intervals called channel. Each of these units will be explained briefly.

3.15.1 Preamplifier

It collects the charge created within the detector by interaction with gamma-radiation and interfaces the detector to the amplifier. It provides a high impedance load for the detector and a low impedance source for the amplifier. The general modes of operation of preamplifiers used in high resolution gamma spectroscopy using semiconductor detector is the charge sensitive (others are current sensitive and voltage sensitive modes). Charge sensitive mode is advantageous in terms of noise performance and the gain is independent of the detector capacitance.

3.15.2 Amplifier

The sharp peaked pulses coming from preamplifiers are not suitable for direct measurement of peak height. For measurement purpose, the ideal pulse would be one gradually approaching a relatively flat top and falling away to the baseline as rapidly as possible. The pile-up of pulses with identical step height produces peak voltages at different heights. The pulse height is proportional to the gamma ray energy absorbed and extraction of information is favorable for rising edges of narrow peaked pulses. This task is accomplished by electronic filtering, also referred to as shaping. Though amplifiers perform shaping, but there can be undesirable consequences associated with this task e.g. impairing resolution.

3.15.3 MCA

The Multichannel Analyzer is a device that separates pulses based on pulse height. Each energy range of pulse height is referred to as a channel. The pulse height is proportional to the energy lost by a gamma photon. Separation of the pulses, based on pulse height, shows the energy spectrum of the gamma rays that are emitted. Multichannel analyzers typically have 4k or 8k channels over an energy range of 0 to 2 MeV (the energy range depends on the amplifier gain setting). The output is a plot of pulse counts versus gamma energy. By analyzing the spectrum of gamma rays emitted, the user can determine the nuclides which caused the gamma pulses. The present day MCA works as a multifunctional device, dealing with many aspects of data analysis, such as collection and sorting pulses, storing and sorting data, data display, data analysis and preparation of data for output. The output is in the form of a display of the number of counts shown on y-axis and the corresponding channel number displayed on x-axis.

3.16 Counting Statistics

The counts (N) of the observed γ lines are numbers resulting from a counting experiment, which are partially superimposed on a high background. This produces an uncertainty of the result which can seriously degrade the precision with which the net peak counts is measured. Counting statistics is applied to estimate this uncertainty which is expressed by the standard deviation of the result.

For any counting experiment the result (N) of which is governed by a Poisson distribution, the standard deviation is

$$\sigma = \sqrt{N} \tag{3.10}$$

The above equation expresses the fact that a repetition of a counting experiment would in about 2/3 of the cases give a result in the range of N ± σ.

For the analysis of a peak without background this is sufficient. But to subtract a background, the Poisson distribution should be approximated by a Gaussian distribution. This can be done without large errors for numbers of counts (N) greater than about 10. In this case,

$$N_{net} = N_{tot} - N_{BG} \tag{3.11}$$

$$\sigma = \sqrt{\sigma_{tot}^2 + \sigma_{BG}^2} = \sqrt{N_{tot} + N_{BG}} \tag{3.12}$$

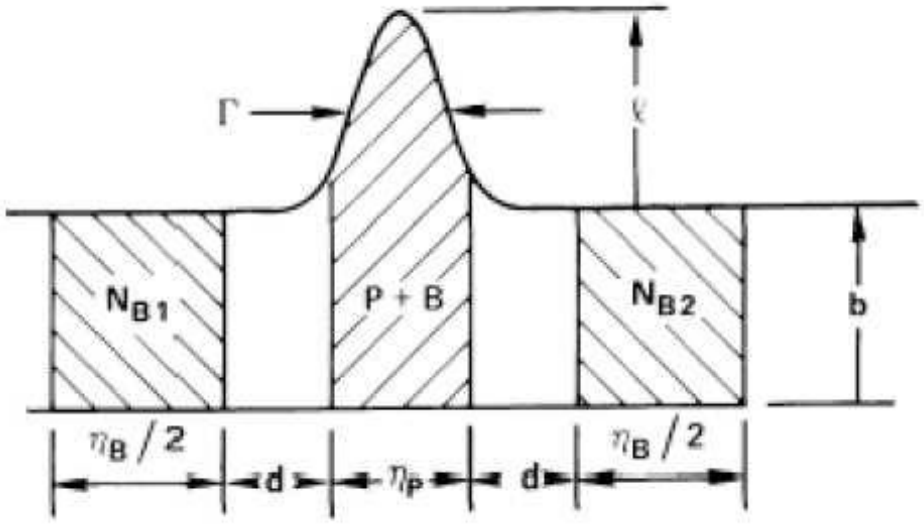

Figure 3.10: Peak and background areas for background subtraction.

In many cases the background has a slope. Therefore the counts in the background areas have to be determined at both sides of the peak and averaged. By such calculation, the value and the statistical error of the activity concentration can be determined.

3.17 Calibrations

The modern digital gamma ray spectrum displays number of pulses measured within small consecutive pulse height ranges. The detector is calibrated to interpret the spectrum in terms of energy rather than channel number or voltage and amount of radionuclides rather than number of pulses. A complicated spectrum analysis may need providing information about peak width variation and shape with energy or channel number. Therefore two main tasks have to be performed

- Energy calibration - the relationship between channel and energy
- Efficiency calibration - the relationship between number of counts and disintegration rate.

3.17.1 Energy calibration

The energy calibration specifies the relationship between peak position in the spectrum (channel number) and the corresponding gamma-ray energy. This is accomplished by measuring the spectrum of a source emitting gamma-rays of precisely known energy and comparing the measured peak position with energy irrespective of the number of nuclides present in the source. For any source, it should be ensured that the calibration energies cover the entire range over which the spectrum is to be used.

In practice, the spectrum should be measured long enough to achieve good statistical precision for the peaks to be used for calibration.

3.17.2 Efficiency calibration

What is meant by efficiency depends on how it is used; three efficiencies can be considered;

- **Relative efficiency:** It is defined as the ratio of absolute efficiency of HPGe detector for counting the 1332.5 keV gamma ray peak area for the ^{60}Co source at 30 cm to the absolute efficiency of 3 in×3 in long NaI(Tl) scintillation detector at the same source to detector distance.
- **Absolute full-peak energy efficiency:** This efficiency relates the peak area in the spectrum to the number of gamma rays emitted by the source. It depends on geometrical arrangement of source and detector.
- **Absolute total efficiency:** This efficiency relates the number of gamma-rays emitted by the source to the number of counts detected anywhere in the spectrum taking into account the full energy peak and all incomplete absorptions represented by Compton continuum.

- **Intrinsic efficiency:** This efficiency relates the counts in the peaks of the spectrum to the number of gamma-rays incident on the detector. This efficiency is independent of source/detector geometry

3.18 Full Energy Peak Efficiency

This parameter is of most significance in practical gamma-spectroscopy and is given by:

$$\varepsilon = R/(A \times I_{\gamma}) \quad (3.13)$$

Where, R is the full energy peak count rate in counts per seconds, A is the source strength in disintegrations per seconds (Bq) and Iγ is the probability of emission of the particular gamma ray being measured.

It is convenient to construct an efficiency curve by measuring many gamma rays and plotting the efficiency versus energy to provide the efficiency data needed by the inverse of equation 3.13 to convert peak area to activity. Generally, point sources emit single gamma rays at low count rates and reasonably large source detector distance. There are several reasons for the irrelevance of such a calibration curve in practice;

- Different source to detector distance
- Different shape of source
- Absorption within the source
- Random summing at high count rate
- True coincident summing at close geometry
- Decay of source during counting
- Electronic timing problems

For environmental measurement that involve a limited set of radionuclides, it would be better to make the measurements relative to a reference standard for each nuclide rather than depending on upon interpolation of a calibration curve. This interpolation introduces extra uncertainties added to those involved in producing a point on the curve. Due to the above mentioned factors, the calibration curve may not be accurate. If the spectrum analysis program requires a calibration curve, then a curve must be created. However, the following correction factors should be considered in using calibration curves;

3.18.1 Dead-time correction

The dead-time correction factor is $(1-R\tau)^{-1}$, where τ is the dead-time value selected for the dead-time module and R is the total count rate above the threshold including the digital overflows. Such factor depends on the sample's count rate.

3.18.2 True coincidence summing

The source of such error is due to the summing of gamma-rays emitted simultaneously from the nucleus. This error is prominent when measurements involving nuclides with complicated decay scheme are conducted. True coincidence summing is geometry dependent and errors are particularly severe when sources are positioned very close to the detector. For this reason, the close geometry efficiency curve requires single-gamma-ray sources.

CHAPTER 4

EXPERIMENTAL SETUP

This chapter discuss about how samples are collected, how samples are prepared for the experiments, what kind of neutron source is used and how characteristics gamma rays from the irradiated samples were measured.

4.1 Sample Collection

For Ytterbium-174 isotopes, we have collected Ytterbium (III) Oxide powder (99.9% pure) from the renowned chemical suppliers Sigma Aldrich (USA) and for Manganese-55 isotopes, we have collected Manganese (IV) Oxide grade-I (99.9% pure) powder sample from the renowned chemical suppliers Jonson Matthey Chemicals Limited (England). We have also collected pure gold foils (Au-197) from Reactor Experiments Incorporation, California (USA) for measuring neutron fluxes during the experiments. Samples and Au foils used in experiment are shown in Figure 4.1.

a b c

Figure 4.1: Samples a) Yb_2O_3 b) MnO_2 and c) Gold Foils.

4.2 Sample Preparation

Powder samples of Ytterbium Oxide (99.99% pure) and Manganese Oxide (99.99% pure) were separately pressed by a hydraulic press at pressure of 5 ton per centimeter square to prepare two pallets of Ytterbium Oxide and two pallets of Manganese Oxide. The diameter of the each pallet was 13mm and thickness 2mm. Then the pellets wrapped in bag by ultraclean polyethylene. After that each sample sandwiched between two thin pure gold foils (diameter =13 mm, thickness=25 μm). The Au-foils were used to monitor beam intensity at both entrance and exit of sample pellet during the irradiation. The details of the samples given in Table-4.1.

Table 4.1: Specifications of investigated materials.

Sample	Weight	Thickness	Diameter	Supplier	Purity	Irradiation Channel
Yb_2O_3	1.29 g	2mm	13mm	Sigma Aldrich (USA)	99.99%	TAS
Yb_2O_3	1.24 g	2mm	13mm	Sigma Aldrich (USA)	99.99%	SAND
MnO_2	1.00 g	2mm	13mm	Jonson Matthey Chemicals Limited (England).	99.99%	TAS
MnO_2	1.00 g	2mm	13mm	Jonson Matthey Chemicals Limited (England).	99.99%	SAND

4.3 Choice of Neutron Source

In the experiments monochromatic neutrons of energies 0.0334eV and 0.0536eV, extracted from the research reactor TRIGA mark-II installed in the premises of Atomic Energy Research Establishment, Savar, Dhaka were used.

4.4 Irradiation of Samples

The Yb targets were irradiated with unidirectional monoenergetic neutrons of 0.0334 eV and 0.0536 eV for 4 h at the outer end position of the last collimator of SAND and TAS, respectively. Similarly, the Mn targets were irradiated with unidirectional monoenergetic neutron beams of energy 0.0334 eV and 0.0536 eV for 180 minutes and for 125 minutes, respectively. The reactor was operated at 2.4 MW power during irradiation of the targets.

4.5. Measurement of Gamma Rays

In our experiments we used high purity germanium gamma ray spectrometry system (25% relative efficiency, 1.9 keV resolution at 1332.5 keV of ^{60}Co) coupled with ORTEC DSPEC jr^{TM} and Maestro data acquisition software to measure the radioactivity induced by ^{174}Yb(n,γ)^{175}Yb , ^{55}Mn(n,γ)^{56}Mn reaction and radionuclide ^{198}Au produced in monitor foils. Hypermet PC software used to analyze the gamma-ray spectra obtained from irradiated samples. Nuclear data related to these experiments are given in Table-4.2.

Table 4.2 Nuclear data for ^{174}Yb(n,γ)^{175}Yb, ^{55}Mn(n,γ)^{56}Mn and ^{197}Au(n,γ)^{198}Au reactions.

Sample	Nuclear reaction	Isotopic abundance	Half-life	Gamma-ray energy (keV)	Gamma-ray emission probability (%)
Yb	^{174}Yb(n,γ)^{175}Yb	31.896	4.185 d	396.3	13.2
				282.5	6.13
Mn	^{55}Mn(n,γ)^{56}Mn	100	2.5789 h	846.76	98.85
Au	^{197}Au(n,γ)^{198}Au	100	161.7 h	411.8	95.62

*Data were taken from NUDAT (2009).

All irradiated samples counted several times with enough time intervals to avoid interferences from gamma lines of unexpected sources and to attain cross sectional values having adequate precision and accuracy. Details of counting of samples are given in Table 4.3. A typical gamma ray spectrum of irradiated Yb_2O_3 and MnO_2 targets are shown in Figure 4.2 and Figure 4.3.

Table 4.3: Details of samples count.

Sample	Gamma-ray energy (keV)	Irradiation channel	Decay time (t_d) sec	Counting time (t_i) sec	Numbers of count (N_p)
Yb_2O_3	396.3	SAND	81645	5519.96	2533
		TAS	840	38552.38	925
	282.5	SAND	81645	5519.96	1354
		TAS	840	38552.38	550
MnO_2	846.76	SAND	11476	3727	37456
		TAS	270	5660.79	4502

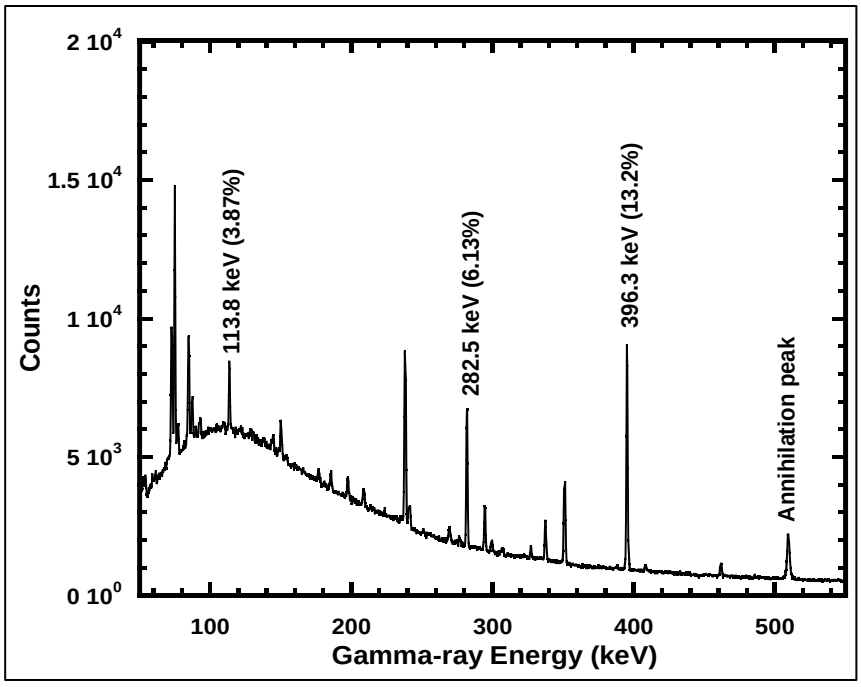

Figure 4.2: A typical gamma ray spectrum for the irradiated Ytterbium Oxide sample.

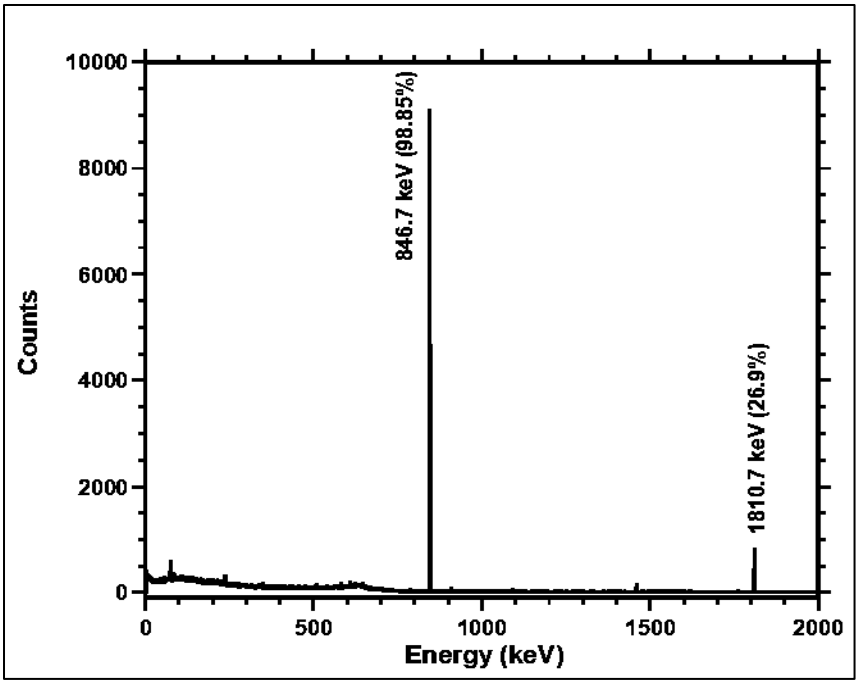

Figure 4.3: A typical gamma ray spectrum for the irradiated Manganese Oxide sample.

CHAPTER 5

EXPERIMENTAL RESULTS AND OBSERVATIONS

5.1 Efficiency Calibration of the Detector

In this study, standard point sources (^{57}Co, ^{60}Co, ^{137}Cs, ^{133}Ba, ^{241}Am and ^{152}Eu) were used to determine the efficiency vs gamma energy curve of HPGe detector by measuring the activities of those sources, placing them individually 30 cm above the detector surface. At 30 cm, effects of random and real coincidences were negligible. The efficiencies of the detector was determined at surface by calculating a normalization factor from the activities of ^{137}Cs (single gamma emitting source) source at 30 cm and surface of the detector. Therefore, the normalization factor was multiplied with the efficiencies of the detector at 30 cm to obtain sum-coincidence free efficiencies at surface of the detector. Energy vs Efficiency curve of HPGe detector is shown in Figure 5.1. The whole efficiencu curve is divided into two parts where lower energy (LE) part is expressed by a fourth order quadratic equations and higher energy (HE) part is expressed by a power equation. These equations are used for calculating efficiencies of the detector at desired gamma-ray energies. The efficiencies of the detector at the desired energies are given in Table 5.1.

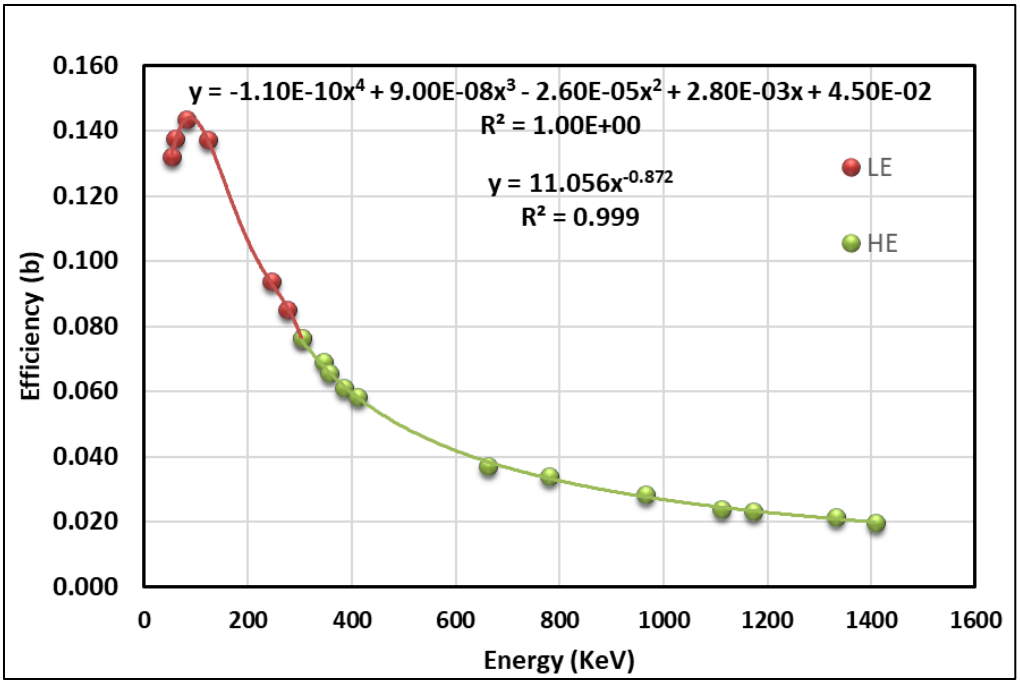

Figure 5.1: Gamma energy vs Efficiency curve of the HPGe detector (LE= Lower energy, HE=Higher energy region).

Table 5.1: Absolute efficiency of the detector at desired energies.

Isotopes	Energy (keV)	Efficiency
Yb-175	282.5	0.0806
Yb-175	396.329	0.0599
Mn-56	846.764	0.0310
Au-198	411.805	0.0554

5.2 Cross Section Calculation of Au-197 (Monitor Gold Foil)

There are no available experimental cross sectional data of $^{197}Au(n,\gamma)^{198}Au$ reaction at our desired energies. So, in order to determine the cross sections of the reaction at our desired energies, we have taken the experimental cross section data reported by Yamamto et el, 1996 and evaluated data from ENDF/B-VIII.0 data library [30-31]. By using those data, we plotted an excitation function by fitting procedure which is shown in Figure 5.2.

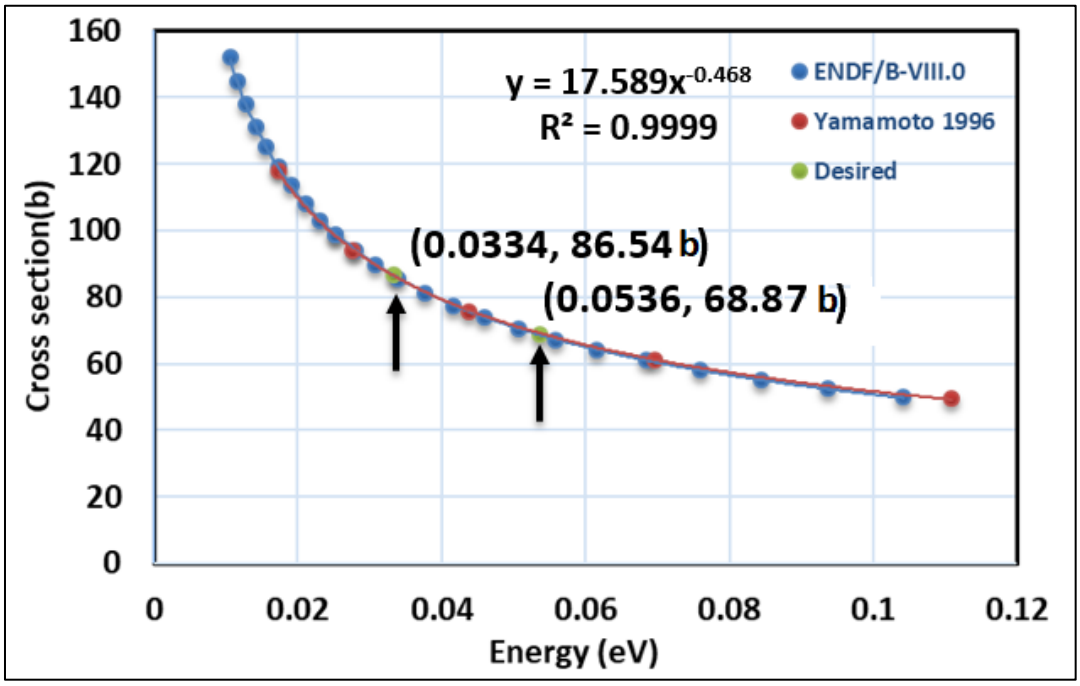

Figure 5. 2 Energy vs Cross section of Au-197.

From the excitation function we developed an equation and by using this equation we calculated cross sections of ^{197}Au (n,γ)^{198}Au reaction at our desired energies of 0.0334 eV and 0.0536 eV. The calculated cross sections are 86.54 b and 68.87 b for the energies of 0.0334 eV and 0.0536 eV, respectively.

5.3 Measurement of Gamma-ray Attenuation

The gamma ray attenuation factor (F_g) in the target sample for a specified gamma-ray energy at certain geometry for the case of cylinder, coaxially positioned with the detector was calculated by considering both the attenuation coefficients for Ytterbium, Manganese and Oxygen elements using the formula below.

$$F_g = \frac{\mu x}{1-e^{-\mu x}} \tag{5.1}$$

Where,

μ = linear attenuation coefficient (cm^{-1}) and

x = Sample thickness (cm)

The mass attenuation coefficient (μ/ρ; cm^2/g) for the elements of Ytterbium, Manganese and Oxygen were taken from the CRC Hand Book of Chemistry and Physics (Lide, 2003) [31]. The total mass attenuation coefficient (cm^2/g) for the compounds (Yb_2O_3 and MnO_2) were transformed into linear attenuation coefficient by multiplying density ρ of the sample. The gamma-ray attenuation factors found in our experiments for the sample pellets are given in the Table 5.2.

Table 5.2: Calculated gamma attenuation factors of the target samples.

Sample	Energy (keV)	F_g
Yb_2O_3	282.5	1.19
	396.3	1.11
MnO_2	846.7	1.03

5.4 Cross Section Determination of $^{174}Yb(n,\gamma)^{175}Yb$

5.4.1 Neutron flux calculation

From the measured activity of ^{198}Au induced in monitor foils, the neutron beam intensities at front and backside of the pellets of Yb_2O_3 at 0.0334 eV and 0.0536 eV energies were calculated by using equation (3.6) given in chapter 3. The details of neutron flux calculation of Yb target samples are given in Table 5.3. Typical spectrums of irradiated Au foil at front and backside of a target are shown in Figure 5.3 and 5.4.

Table 5.3: Average neutron flux for Yb_2O_3 samples.

Sample	Sample Position	Neutron Energy (eV)	Front side flux $(cm^{-2}s^{-1})$	Backside flux $(cm^{-2}s^{-1})$	Average Flux $(cm^{-2}s^{-1})$
Yb_2O_3	SAND	0.0334	(4.66 ±0.21)x10^4	(3.78±0.20)x10^4	(4.22±0.29)x10^4
	TAS	0.0536	(8.28 ±0.41)x10^3	(6.39±0.27)x10^3	(6.89±0.27)x10^3

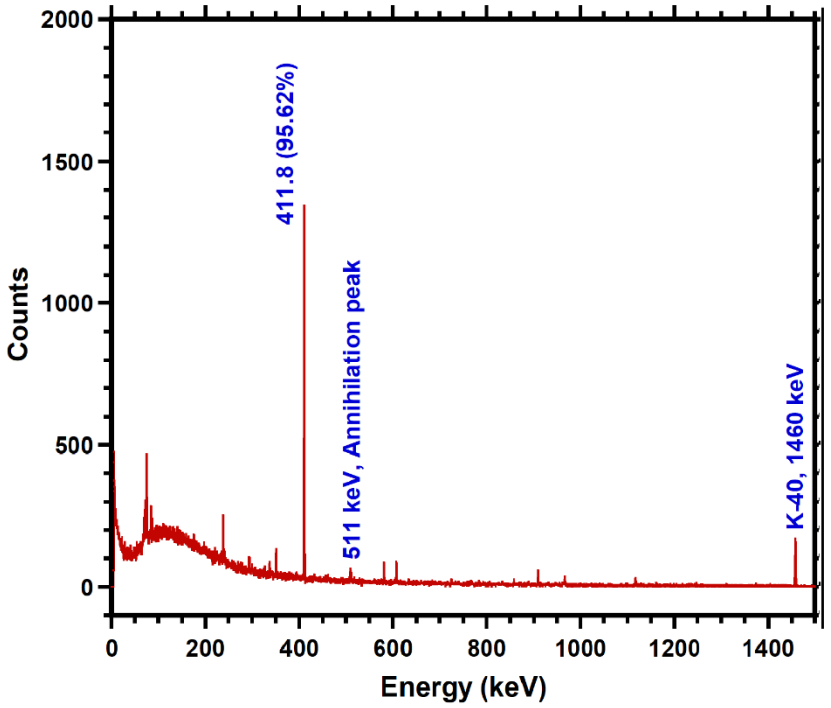

Figure 5.3: Gamma-ray spectrum of an irradiated Au-foil (Front side).

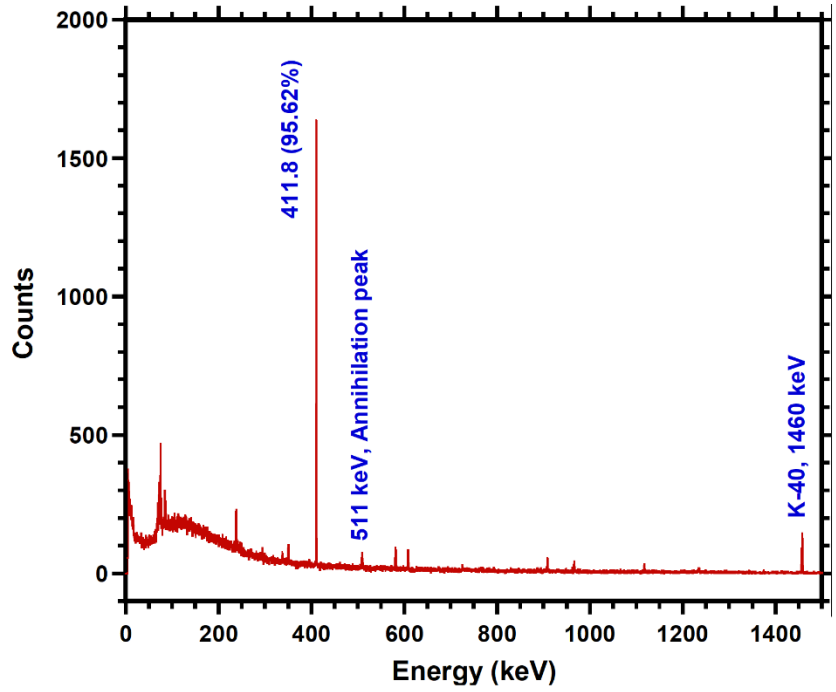

Figure 5.4: Gamma-ray spectrum of an irradiated Au-foil (backside).

5.4.2 Neutron attenuation at the sample targets

For 0.0334 eV neutrons, the neutron beam intensity at front and rear side were $(4.66 \pm 0.21)\times10^4$ and $(3.78\pm0.20)\times10^4$ $cm^{-2}s^{-1}$, respectively. Therefore, for Yb target, attenuation of neutrons at the pellet was 19% of the entering beam intensity. For 0.0536 eV neutrons, the obtained neutron beam intensity at front and rear side were $(8.28 \pm 0.41)\times10^3$ and $(6.39 \pm 0.27)\times10^3$ $cm^{-2}s^{-1}$, respectively. Therefore, attenuation of neutrons at the pellet for this energy was 22.8% of the entering beam intensity. The average of the neutron beam intensity at front and rear side of the Yb target was considered as effective neutron beam intensity due to neutron attenuation of the target. The average neutron beam intensity is given in Table 5.3.

5.4.3 Calculation of uncertainties associated with determined cross-section

The overall uncertainty of the resultant cross section of our experiments was determined by taking the square root of the quadratic sum of the separate uncertainties. Sources of uncertainties considered for overall uncertainty calculation in the measured cross section are given in the Table 5.4.

Table 5.4: Overall uncertainties in the measured cross section of $^{174}Yb(n,\gamma)^{175}Yb$ reaction.

Source of error	Uncertainty (%)
Statistical uncertainty due to gamma-counting	2-4
Decay branching ratio	3.0
Half life	0.03
Efficiency calibration	4.0
Sample mass	0.01
Isotopic abundance	1.26
Total uncertainty	6.55

5.4.4 Cross sections of $^{174}Yb(n,\gamma)^{175}Yb$ reaction at 0.0334 eV and 0.0536 eV energies

After considering all correction factors such as detector efficiency, neutron and gamma ray attenuation, the measured cross section of $^{174}Yb(n,\gamma)^{175}Yb$ reaction at 0.0334 eV and 0.0536 eV energies are 56.8 ± 3.7 b and 44.2 ± 2.6 b, respectively. The experimental cross sections data along with some original experimental data are given in Table 5.5. The normalized values of the original data by using Miyahara et al., 1994 absolute gamma-ray emission probabilities are also given in Table 5.5. The measured data at 0.0334 eV energy is 45.4% less than the theoretically evaluated JEFF-3.3 data and 5.7 % less than the evaluated data of ROSFOND-2010. We also compared our data with data of N. Belouadah et al. (2014) at 0.0372 eV and found our data is 9% lower than their value. Our data at 0.0334 eV is in agreement with evaluated data of JENDL-4.0 and ENDF/B-VIII.0. The experimental data at 0.0536 eV energy is 46.2 % less than the theoretically evaluated JEFF-3.3 data and 6.9 % less than the evaluated data of ROSFOND-2010. This experimental data is also in agreement with evaluated data of JENDL-4.0 and ENDF/B-VIII.0.

Table 5.5: Experimental cross sections for the $^{174}Yb(n,\gamma)^{175}Yb$ reaction.

Year	References	Neutron energy (eV)	Cross section for the $^{174}Yb(n,\gamma)^{175}Yb$ reaction in barn				Methods
			Original Papers	Recommended	Compilations	Normalized	
2019	This work	0.0536	44.2±2.6				Act. meth .θ= 31.8%; I_γ = 13.2%
		0.0334	56.8 ± 3.7				Act. meth .θ= 31.8%; I_γ = 13.2%
		0.0253	64.8±2.9				Extrapolated*
2014	Belouadah et al.	0.0372	59.07±2.3				Act. meth .θ= 31.8%; I_γ = 13.2%
2014	Belouadah et al.	0.0253	71.6 ± 2.7				Expected 1/v cross section
2008	Karadag and Yucel	0.0253	126.5± 6.6			126.5 ± 6.6	Act. meth. Θ=31.84% I_γ =13.2%
2006	Mughabghab	0.0253		63.2 ± 1.5	63.2 ± 1.5		
2003	De Corte	0.0253			63.4 ± 1.7		
1997	Kafala et al.	0.0253	131 ± 6		61 ± 2.7		Act. meth. Norm to I_γ (396) =13.101
1996	Simonits et al.	0.0253		62.5 ± 0.75			
1995	IAEA NDS NUDAT	0.0253			69.4 ± 5		From BNL-325
1989	De Corte and Simonits	0.0253	128 ± 8			61.65 ± 3.8	Act. meth. I_γ (396) = 6.31%, Norm to I_γ (396) = 13.101
1987	IAEA	0.0253			65 ± 5		
1985	De Corte et al.	0.0253	128.8± 1.9			62.04 ± 0.92	
1978	Heft	0.0253	108 ± 4			57.54 ± 2.13	Act. meth. Norm to I_γ (396) = 13.101
1977	Walker et al				65		
1976	Erdtmann				65 ± 5		
1970	Sims and Juhnke	0.0253	141 ± 2			64.58 ± 0.92	Act. meth. Norm to I_γ(396)=13.101
1968	Mughabghab and Cherien	0.0253	65 ± 5				Transmission meth.; 98.97% ^{174}Yb; σ_{tot}=142b, $\sigma_{scatter}$=77b
1968	Holden and Walker				65		
1963	Alexander and Brinckmann	0.0253	46 ± 4				Act. Meth.
1965	Walker	0.0253	72 ± 6				

3.5 Cross Section Determination for $^{55}Mn(n,\gamma)^{56}Mn$ Reaction

3.5.1 Neutron flux calculation

From the measured activity of ^{198}Au induced in monitor foils, the neutron beam intensities of front and backside of the MnO_2 pellets at 0.0334 eV and 0.0536 eV energies are given in Table 5.6.

Table 5.6: Neutron flux at MnO_2 samples.

Sample	Sample Position	Neutron Energy (eV)	Front side flux $(cm^{-2}s^{-1})$	Backside flux $(cm^{-2}s^{-1})$	Average Flux $(cm^{-2}s^{-1})$
MnO_2	SAND	0.0334	(3.25±0.1)x10^4	(2.54±0.02)x10^4	(2.9±0.01)x10^4
	TAS	0.0536	(8.28±0.25)x10^3	(5.49±0.17)x10^3	(6.89±0.30)x10^3

5.5.2 Neutron attenuation calculation

For 0.0334 eV neutrons, the front and backside neutron fluxes of the pellet were measured (3.25±0.1) x10^4 and (2.54±0.08) x10^4 $cm^{-2}s^{-1}$, respectively. Similarly, for 0.0536 eV neutron energy, the front and backside neutron fluxes of the pallet were, (8.28±0.25) x10^3 and (5.49±0.17) x10^3 $cm^{-2}s^{-1}$, respectively. The average of the neutron fluxes at front and backside of the MnO_2 target considered as effective neutron flux for neutron attenuation in the target. For the Mn targets, the effective neutron fluxes for 0.0334 eV and 0.0536 eV energies were (2.89±0.13) x10^4 and (6.89±0.30)x10^3 $cm^{-2}s^{-1}$, respectively.

5.5.3 Calculation of uncertainties associated with determined cross-section

The overall uncertainty of the resultant cross section of our experiments was determined by taking the square root of the quadratic sum of the separate uncertainties. Sources of uncertainties considered for overall uncertainty calculation in the measured cross section are given in the Table 5.7.

Table 5.7: Overall uncertainties in the measured cross section of $^{55}Mn(n,\gamma)^{56}Mn$ reaction.

Source of error	Uncertainty (%)
Statistical uncertainty due to gamma-counting	0.52
Peak area analysis	2.0
Half life	0.01
Efficiency calibration	4.0
Sample mass	0.01
Isotopic abundance	0.016
Self-shielding factor	0.01
Neutron flux	3.0
Decay branching ratio	Negligible
Total uncertainty	5.4

5.5.4 Cross sections of $^{55}Mn(n,\gamma)^{56}Mn$ reaction at 0.0334 eV and 0.0536 eV energies

After considering all correction factors such as detector efficiency, neutron and gamma ray attenuation, the measured cross section of $^{55}Mn(n,\gamma)^{56}Mn$ reaction at 0.0334 eV and 0.0536 eV energies are 11.07 ± 0.6 b and 09.03±0.49 b, respectively. The obtained cross section values along with available literature data are given in Table 5.8. It is observed that our experimental data are in agreement with the theoretically evaluated data libraries such as ENDF/B-VIII, JENDL-4.0, ROSFOND-2010 and JEFF-3.3 within uncertainty limit (Table 5.8).

Table 5.8: Experimental cross sections for the $^{55}Mn(n,\gamma)^{56}Mn$ reaction.

Year	References	Neutron energy (eV)	Literature value (b)
2019	This work	0.0536	09.03±0.49
		0.0334	11.07±0.60
		0.0253*	12.93±0.99
1946	Coltman	0.0253	10.7±0.2
1950	Corlmer	0.0253	12.8±0.8
1950	Harris	0.0253	12.3
1951	Grimland	0.0253	12.4±0.2
1957	Cumins	0.0253	13.2±0.2
1963	Huttel	0.0253	13.3±0.08
1970	Hogg et al.	0.0253	13.5±0.5
1976	Adib et al.	0.0253	13.64±0.19
1981	Mughabghab	0.0253	13.36±0.5

CHAPTER 6

DISCUSSION ON RESULTS AND RELEVANCE

This chapter explain and evaluate the findings of our research and shows how it relates to our literature review and research questions.

6.1 Discussion on Cross Section of $^{174}Yb(n,\gamma)^{175}Yb$ Reaction

The neutron capture cross section values for the $^{174}Yb(n,\gamma)^{175}Yb$ reaction measured in this work at new energies of 0.0334 eV and 0.0536 eV are 56.8±3.7 b and 44.2±2.6 b, respectively. As far as we know, there is no experimental neutron capture cross section data available at these energies for the studied reaction. In this study, two independent gamma-rays of 282.5 keV and 396.3 keV from the decay of ^{175}Yb were considered to measure activity of the radionuclide. The neutron capture cross section values measured separately for these gamma lines are very close to each other. The resultant cross sections at 0.0334 eV and 0.0536 eV were individually extrapolated to the values at energy of 0.0253 eV by following the 1/v dependence in the thermal region assuming that the Westcott factor of the $^{174}Yb(n,\gamma)^{175}Yb$ reaction cross section is around to the unity. The results are 65.28±4.29 b and 64.38±3.86 b. These results are in good agreement to each other. The average of these two values 64.8±2.9 b at 0.0253 eV energy is calculated and compared with the results of previous works in the literature.

The compiled data and the recommended ones by Mughabghab (2006) and Simonits et al. (1996) of the thermal neutron capture cross section for the $^{174}Yb(n,\gamma)^{175}Yb$ reaction are also given in the Table 5.5. Most of these values are given at 0.0253 eV neutron energy. The measured cross sections in this work along with the normalized experimental values, the recommended value by Mughabghab (2006) and Simonits et al. (1996) for the 0.0253 eV

neutron energy and the evaluated data in the ENDF/B-VIII, JENDL-4.0, JEFF-3.3 and ROSFOND-2010 files are plotted in Figure 6.1.

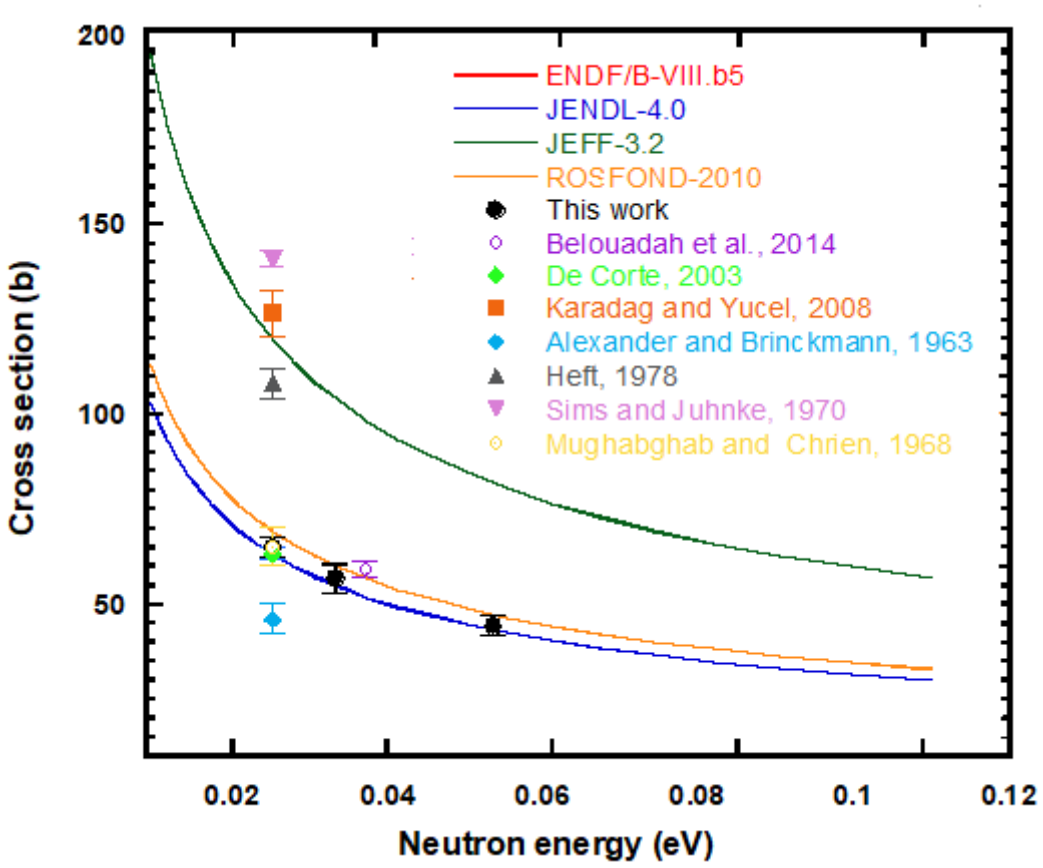

Figure 6.1: Thermal neutron capture cross section versus neutron energy for the $^{174}Yb(n,\gamma)^{175}Yb$ reaction.

The values calculated in this experiment at 0.0334 eV and 0.0536 eV are very close to the evaluated data curves (Figure 6.1) of ENDF/B-VIII and JENDL-4 library based on calculation using the 1/v relationship. ROSFOND -2010 data libraries are also in agreement with the measured values within the uncertainties reported with the measured values. However, experimental values in this work at 0.0334 eV and 0.0536 eV are not in agreement with the JEFF-3.3 data libraries. Our experimental cross section data at 0.0334 eV is 45.4% less and at 0.0536 eV it is 46.2% less than the theoretically evaluated JEFF-3.3 data. If we extrapolate our

experimental data at 0.0334 eV to 0.0372 eV and compare with the experimental data obtained by Belouadah et al. (2014) at 0.0372 eV, we found that our data is 9% lower than their reported data.

As given in Table 5.5, the measured capture cross section at 0.0253 eV neutron energy for the $^{174}Yb(n,\gamma)^{175}Yb$ reaction reported in the literature show large discrepancies between 46 and 141 b. However, Kafala et al. (1997), De Corte and Simonits (1989) and De Corte et al. (1985) have used the K_0 activation method and their values of thermal cross section at 0.0253 eV were reported to be $\sigma = (131 \pm 6)$ b, $\sigma = (128 \pm 8)$ b and $\sigma = (130 \pm 4)$ b, respectively. Heft (1978) and Walker (1956) have also used the activation method and calculated the average capture cross section over the thermal neutrons spectrum they obtained $\sigma = (108 \pm 4)$ b and (72 ± 6) b, respectively. Sims and Juhnke, 1970; Alexander and Brinckmann, 1963 found a value, averaged over a Maxewellian spectrum, of $\sigma = (141 \pm 2)$ b and (46 ± 4) by using gamma-ray emission probability value around 6% (Table 5.5).

On the other hand, the data obtained by the method of transmission (Mughabghab and Chrien, 1968) ($\sigma = 65 \pm 5$b) is in good agreement with the values recommended by Mughabghab (2006) ($\sigma = 63.2 \pm 1.5$ b) and Simonits et al. ($\sigma = 62.5 \pm 0.75$ b). Simonits et al. (1996) attributed these discrepancies are mainly due to the choice of the absolute gamma-ray emission probabilities of ^{I75}Yb, used in the activation measurements. However, the measurement methods, the reference reaction, and the irradiation neutrons source can be also be sources of disagreement between different experimental data. The discrepancies among the data obtained by activation method can be explained by the used method. To obtain data at 0.0253 eV by activation method, they used Cd cut-off technique. The Cd Cut-off method needs the separation of the thermal neutron flux from the epithermal neutrons and requires several parameters that can be

the sources of uncertainty [17]. It should be noted that the method applied in this experiment is more accurate and delivers directly monochromatic neutrons beam of 0.0334 eV and 0.0536 eV.

If we closely analyze the available literature data at 0.0253 eV for the studied reaction, it is observed that one group of researchers have determined cross section values between 108 and 141 b considering a value around 6% for the gamma-ray emission probability, on the other hand a second group among the recommended and compiled data show values between σ = 62.5 and σ = 69.4 b considering the recommended gamma-ray emission probability around 13.1% [33]. Our reported cross section data (64.8±2.9 b) at 0.0253 eV is in good agreement with the data measured by the method of transmission (Mughabghab and Chrien, 1968) as well as with the values obtained by second group of researchers. Moreover, if experimental values of the first group were normalized with the use of the gamma-ray emission probability recommended by Simonits et al. (1996), we found that the normalized values agree with those of the second group.

6.2 Discussion on Cross Section of $^{55}Mn(n,\gamma)^{56}Mn$ Reaction

The resultant cross sections in this study for the reaction $^{55}Mn(n,\gamma)^{56}Mn$ at 0.0334 eV and 0.0536 eV are 11.07±0.6 b and 09.03±0.49 b, respectively. As far as we know, there are no experimental data available for the $^{55}Mn(n,\gamma)^{56}Mn$ reaction at our studied energies. The characteristic gamma ray of 846.8 keV emits by the radionuclide ^{56}Mn was used to determine the activity. The gamma-ray attenuation factor for the target pellets of MnO_2 calculated 1.03 for the 846.8 keV characteristic gamma ray energies emitted from the decay of ^{56}Mn radionuclide.

The average of the neutron fluxes at front and backside of the Mn target considered as effective neutron flux for neutron attenuation in the target. For the Mn targets, the effective neutron fluxes for 0.0334 eV and 0.0536 eV energies were (2.89±0.13) $x10^4$ and (6.89±0.30) $x10^3$ $cm^{-2}s^{-1}$ respectively. By following 1/v assumption in the thermal region, the resultant cross sections at 0.0334 eV and 0.0536 eV extrapolated at average thermal energy 0.0253 eV. The extrapolated results are 12.72±0.69 b and 13.14±0.71 b and the average of those two results 12.93±0.99 b at 0.0253 eV calculated to compare with results of previous works. The experimental determined cross section data and other available literature data are plotted in Figure 6.2.

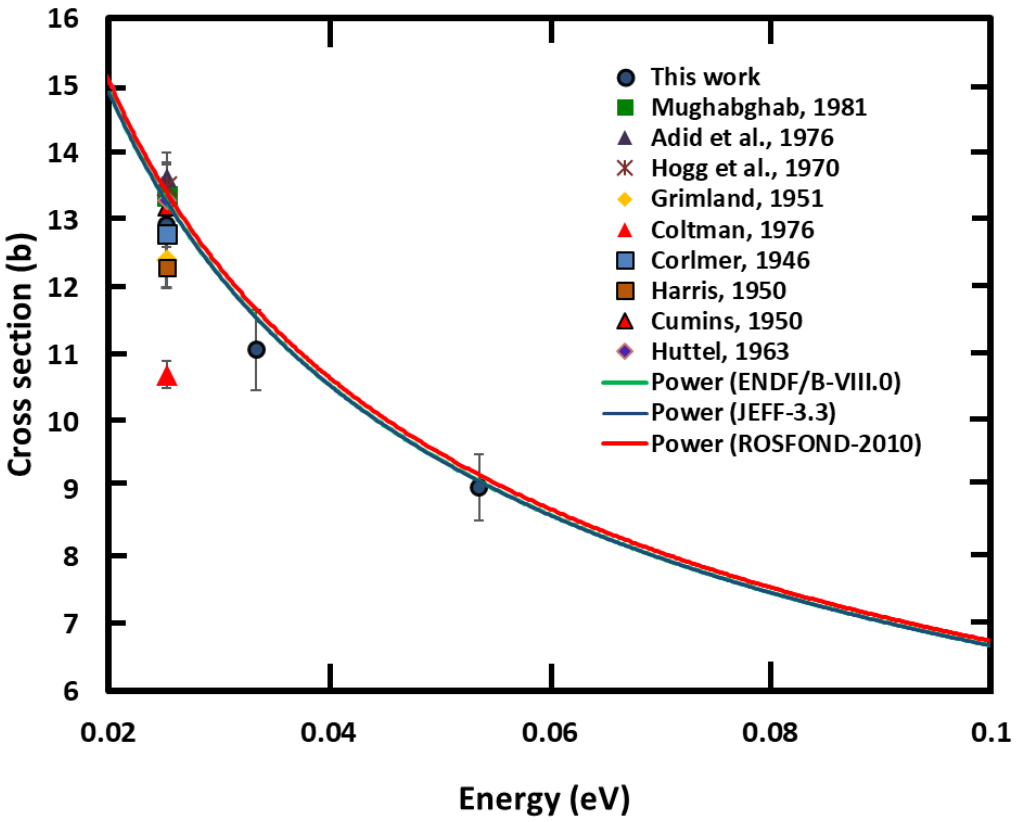

Figure 6.2: Thermal neutron capture cross section versus neutron energy for the $^{55}Mn(n,\gamma)^{56}Mn$ reaction.

All reported literature data are at average thermal neutron energy of 0.0253 eV. The reported data varies within 10.7 b to 13.64 b. Our extrapolated data (12.93±0.99 b) at 0.0253 eV based on experimental results is 20.84%, 4.27%, 5.31% and 1% higher than the data reported by the Coltman, 1946 (10.7±0.2 b), Grimland, 1951 (12.4±0.2 b), Harris, 1950 (12.3 b) and Corlmer, 1950 (12.8±0.8 b) respectively . On the other hand the extrapolated data (12.93±0.99 b) is 3.22%, 5.21% ,4.22%, 2.02% and 2.8% lower than the data reported by the Mughabghab, 1981 (13.36±0.5 b), Adib et al.,1976 (13.64±0.19 b), Hogg et al., 1970 (13.5±0.5 b), Cumins, 1957 (13.2±0.2 b) and Huttel, 1963 (13.3±0.08 b) respectively. We also compared our experimental data with the evaluated data library of ENDF/B-VIII.0, JEFF-3.3 and ROSFOND-2010 data libraries and found that within uncertainty limit our experimental results are consistent with those data libraries (Figure 6.2).

CHAPTER 7

CONCLUSIONS AND FUTURE WORK

7.1 Conclusions

The neutron capture cross sections of the reactions $^{174}Yb(n,\gamma)^{175}Yb$ and $^{55}Mn(n,\gamma)^{56}Mn$ at neutron energies of 0.0334 eV and 0.0536 eV were determined for the first time by using monochromatic neutrons from TRIGA MARK-II research reactor. The experimental cross sections for the $^{174}Yb(n,\gamma)^{175}Yb$ reaction at 0.0334 eV and 0.0536 eV are amounted to 56.8 ± 3.7 b and 44.2 ± 2.6 b, respectively. The obtained experimental values at 0.0334 eV and 0.0536 eV are in agreement with the theoretically evaluated data libraries of JENDL-4.0 and ENDF/B-VIII. However, our extrapolated data at 0.0253 eV is 45% less than the theoretically evaluated JEFF-3.3 data. Our extrapolated data at 0.0253 eV was compared with available literature data, which enabled us to resolve discrepancies of the data at thermal energy region for this reaction. Since the data obtained from this study at 0.0253 eV (64.8±2.9 b) are in good agreement with JENDL-4.0 and ENDF/B-VIII data libraries, this study validate the excitation functions of these two data libraries at thermal energy region. However, data obtained from this study do not support the JEFF-3-3 data library.

The determined experimental cross sections for the $^{55}Mn(n,\gamma)^{56}Mn$ reaction at 0.0334 eV and 0.0536 eV are 11.07±0.6 b and 09.03±0.49 b, respectively. The resultant cross sections obtained from this study are consistent with those data libraries within the uncertainty limits.

The experimental data on Yb target obtained from this study will be useful to measure activity distribution, therapeutic radioisotope production and studies related to the interaction of neutrons with matter, whereas the obtained data on Mn target will be used in monitor reaction

and developing nuclear grade structural material for future reactor technology. This study will also encourage cross-section measurements for various reactions, at different energies in the thermal energy region, at our laboratory as well as at many places in the world where neutron diffractometer and spectrometer are installed.

7.2 Recommendation for Future Work

- Some more targets related to neuclear reactor technology will be studied in future.
- The target irradiation system at radial beam ports of Center for Research Reactor (CRR) will be simulated using Monte Carlo N-Particle Transport Code (MCNP).

REFERENCES

[1] Mould, R.F., 1995. The early history of x-ray diagnosis with emphasis on the contributions of physics 1895-1915. *Physics in Medicine & Biology*, *40*(11), p.1741.

[2] Obložinský, P., Herman, M. and Mughabghab, S.F., 2010. Evaluated nuclear data. *Handbook of Nuclear Engineering*, pp.83-187.

[3] Rullhusen, P., 2006. *Nuclear Data Needs for Generation IV Nuclear Energy Systems: Proceedings of the International Workshop, Antwerpen, Belgium, 5-7 April 2005*. World Scientific.

[4] Pandey, B., Agrawal, H.M. and Pepelnik, R., 2014. Neutron activation cross-sections for Ytterbium isotopes at (14.6±0.3) MeV. *Applied Radiation and Isotopes*, *85*, pp.128-132.

[5] Karadag, M. and Yücel, H., 2008. Measurement of thermal neutron cross-section and resonance integral for the ^{174}Yb (n, γ) ^{175}Yb reaction by the cadmium ratio method. *Nuclear Instruments and Methods in Physics Research Section B: Beam Interactions with Materials and Atoms*, *266*(11), pp.2549-2555.

[6] Qaim, S.M., 2001. Nuclear data relevant to the production and application of diagnostic radionuclide. *Radiochimica Acta*, *89*(4-5), pp.223-334.

[7] Simonits, A., De Corte, F. and De Wispelaere, A., 1996. The ^{174}Yb (n, γ) ^{175}Yb reaction: a convincing new argument for k0-standardization in absolute neutron activation analysis. *Applied radiation and isotopes*, *47*(4), pp.389-394.

[8] Schuman, R.P., 1971. *The Radiochemistry of Manganese*. National Academies.

[9] Rullhusen, P., 2006. *Nuclear Data Needs for Generation IV Nuclear Energy Systems: Proceedings of the International Workshop, Antwerpen, Belgium, 5-7 April 2005*. World Scientific.

[10] Davis, W., 2012. Reactor pressure vessels: *Metallurgy and Fabrication. Atomic Power Review*.

[11] Vansola, V., Mukherjee, S., Naik, H., Suryanarayana, S.V., Ghosh, R., Badwar, S., Lawriniang, B.M. and Sheela, Y.S., 2016. Determination of ^{55}Mn (n, γ) ^{56}Mn reaction cross-

section at the neutron energies of 1.12, 2.12, 3.12 and 4.12 MeV. *Radiochimica Acta*, *104*(11), pp.749-755.

[12] Guber, K., Paradela, C., Heyse, J., Kopecky, S., Schillebeeckx, P. and Siegler, P., 2017. Neutron nuclear data measurements for criticality safety. In *EPJ Web of Conferences* (Vol. 146, p. 11020). EDP Sciences.

[13] De Corte, F., 2003. The updated NAA nuclear data library derived from the Y2K k0-database. *Journal of radioanalytical and nuclear chemistry*, *257*(3), pp.493-499.

[14] Simonits, A., De Corte, F. and De Wispelaere, A., 1996. The ^{174}Yb (n, γ) ^{175}Yb reaction: a convincing new argument for k0-standardization in absolute neutron activation analysis. *Applied radiation and isotopes*, *47*(4), pp.389-394.

[15] Mughabghab, S.F., 2012. *Neutron Cross Sections: Neutron Resonance Parameters and Thermal Cross Sections Part B: Z= 61-100* (Vol. 1). Academic press.

[16] Mughabghab, S.F., 2006. *Atlas of Neutron Resonances: Resonance Parameters and Thermal Cross Sections. Z= 1-100*. Elsevier.

[17] Holden, N.E., Walker, F.W., 1968. Chart of the Nuclides, 10th ed., General Electric Co., Schenectady, NY.

[18] Afroze, N., Uddin, M.S., Hossain, S.M., Islam, M.A., Shariff, M.A., Zakaria, A.K.M., Datta, T.K. and Islam, S.A., 2014. Experimental cross section of the ^{71}Ga (n, γ) ^{72}Ga reaction at 0.0334 eV energy. *Nuclear Instruments and Methods in Physics Research Section B: Beam Interactions with Materials and Atoms*, *336*, pp.1-5.

[19] Belouadah, N., M. Belgaid, and T. Zidi. "Neutron capture cross section measurement for the ^{174}Yb (n, γ) ^{175}Yb reaction at 0.0372 eV energy." *Annals of Nuclear Energy* 64 (2014): 264-269.

[20] Sims, G. H. E., Juhnke, D. G., 1970. The thermal neutron capture cross sections and resonance capture integrals of ^{44}Ca, ^{62}Ni, ^{168}Yb, ^{174}Yb ^{169}Tm and ^{203}Tl. *Journal of Inorganic Nuclear Chemitry*, 32(9), pp.2839-2844.

[21] Heft, R. e., 1978. A consistent set of nuclear parameter values for absolute neutron activation analysis. InProc. Mayag Conf. (vol.495).

[22] Coltman, J.W. and Goldhaber, M., 1946. Capture cross sections for slow neutrons. *Physical Review*, *69*(9-10), p.411. [20] Hogg, C.H., Wilson, W.L., 1970, Idaho Report IN-1317 53.

[23] Adib, M., Abdel-Kawy, A., Faragalla, S., Sadek, S., Salama, M. and Hamouda, I., 1976. Measurements of the total neutron cross-section and manganese in the energy range 1.8 meV to 1.8 eV. *Atomkernenergie*, *27*(2), pp.117-119.

[24] Griraeland, B. et al., 1951, Compt. Rend. 23J2 2089.

[25] Hůttel, G., Liewers, P., 1963, Kernenergie 6 336.

[26] Cummins, J.D., Spurway, A. H., 1957, Harwell Report AERE R/M 100.

[27] Colmer, F.C.W., Littler, D.J., 1950, "roc. Phys. Soc. London A63 1175.

[28] Harris, S.P., Muehlhause, C.O., Rasmussen, S., Schroeder, H.P. and Thomas, G.E., 1950. Pile neutron absorption cross sections. *Physical Review*, *80*(3), p.342.

[29] C.H. Hogg, W.L. Wilson., 1970, Idaho Report IN-1317 53.

[30] Evans, R.D. and Evans, R.D., 1955. The atomic nucleus.

[31] Yamamoto, S., Kobayashi, K. and Fujita, Y., 1996. Application of BGO Scintillators to Absolute Measurement of Neutron Capture Cross Sections between 0.01 eV and 10eV. *Journal of nuclear science and technology*, *33*(11), pp.815-820.

[32] Brown, D.A., Chadwick, M.B., Capote, R., Kahler, A.C., Trkov, A., Herman, M.W., Sonzogni, A.A., Danon, Y., Carlson, A.D., Dunn, M. and Smith, D.L., 2018. ENDF/B-VIII. 0: the 8th major release of the nuclear reaction data library with CIELO-project cross sections, new standards and thermal scattering data. *Nuclear Data Sheets*, *148*, pp.1-142.

[33] Lide, D.R. ed., 2004. *CRC handbook of chemistry and physics* (Vol. 85). CRC press.

[34] Miyahara, H., Matumoto, H. and Mori, C., 1994. Precise measurement of the gamma-ray emission probability for 175Yb. *Applied radiation and isotopes*, *45*(2), pp.219-223.

APPENDIX A

Calculation of Neutron Flux for Yb sample at SAND (0.0334 eV)

Here,

Mass of front side Au foil M = 0.06101 g

Mass of backside Au foil M = 0.06018 g

Cross section of Au-197 at 0.0334 eV $\sigma = 8.6542\times10^{-23}$ cm^2

Avogadro's number $N_A = 6.02213 \times 10^{23}$

Isotropic abundance(θ) for Au-197 = 1

Gamma ray intensity Iγ = 0.9562

Atomic weight of Au W = 196.967

Efficiency of the detector at 411.805 KeV energy Ɛ= 0.0554

Half-life of Au-198 $T_{1/2}$ = 2.697 days = 233020.8 sec

Decay constant $\lambda = \frac{0.693}{T_{1/2}} = 2.97 \times 10^{-6}$

Irradiation time t_i = 14220 sec

Irradiation factor $F_i = \{1 - e^{-\lambda t_i}\}$

$= \{1 - e^{-(2.97\times10^{-6}\times14220)}\}$

= 0.04141

Decay time for front side foil t_d = 66949 sec

Decay time for backside foil t_d = 81645 sec

Decay factor for front side foil $F_d = e^{-\lambda t_d}$

$= e^{-(2.97\times10^{-6}\times66949)}$

= 0.819

Decay factor for backside foil $F_d = e^{-\lambda t_d}$

$= e^{-(2.97\times10^{-6}\times81645)}$

= 0.784

Number of count for front side foil N_p = 5392

Counting time for front side foil t_c = 4018.41 sec

Counting rate for front foil R = $\frac{5392}{4018.41}$

= 1.342 sec^{-1}

Activity for front foil A = R/ $I_\gamma \varepsilon$

$= \frac{1.342}{0.9562 \times 0.0554}$ Bq

= 25.33 Bq

Counting factor for front side foil,

$F_c = \left\{\frac{1-e^{-\lambda t_c}}{\lambda t_c}\right\}$

$= \left\{\frac{1 - e^{-(2.97 \times 10^{-6} \times 4018.41)}}{(2.97 \times 10^{-6} \times 4018.41)}\right\}$

= 0.994

Number of count for front side foil N_p = 4457

Counting time for backside foil t_c = 4338.57 sec

Counting rate for backside foil R = $\frac{4457}{4338.57}$

= 0.9212

A = R/ $I_\gamma \varepsilon$

$= \frac{0.9212}{0.9562 \times 0.0554}$ Bq

= 17.38 Bq

Counting factor for backside foil,

$F_c = \left\{\frac{1-e^{-\lambda t_c}}{\lambda t_c}\right\}$

$= \left\{\frac{1 - e^{-(2.97 \times 10^{-6} \times 3338.57)}}{(2.97 \times 10^{-6} \times 3338.57)}\right\}$

= 0.994

From the equation (3.7), we found

$$\Phi = \frac{AW}{N_A \sigma M \theta \, Fi \times F_d \times F_c}$$

So, neutron flux at front side,

$$\Phi_f = \frac{AW}{N_A \sigma M \theta \, Fi \times F_d \times F_c}$$

$$= \frac{25.33 \times 196.967}{6.02213 \times 10^{23} \times 8.654 \times 10^{-23} \times 0.06018 \times 1 \times 0.0414 \times 0.819 \times 0.994}$$

$$= 4.66 \times 10^4 \text{ cm}^{-2}\text{s}^{-1}$$

So, neutron flux at backside,

$$\Phi_b = \frac{AW}{N_A \sigma M \theta \, Fi \times F_d \times F_c}$$

$$= \frac{17.38 \times 196.967}{6.02213 \times 10^{23} \times 8.654 \times 10^{-23} \times 0.06101 \times 1 \times 0.0414 \times 0.784 \times 0.994}$$

$$= 3.78 \times 10^4 \text{ cm}^{-2}\text{s}^{-1}$$

Average neutron flux at Yb sample pellet at SAND $= \frac{(4.66 \times 10^4) + (3.78 \times 10^4)}{2}$

$$= 4.22 \times 10^4 \text{ cm}^{-2}\text{s}^{-1}$$

APPENDIX B

List of Publications and Conference Presentations

Publications:

[1] **Zaved, M.M.,** Islam, M.A. and Hossain, A., 2020. Experimental cross sections of the 174Yb (n, γ) 175Yb reaction at new energies of 0.0334 eV and 0.0536 eV. Radiation Physics and Chemistry, 166, p.108471.

Conference Presentations:

[1] Zaved, M.M., Islam, M. A., Rahman, M., Hossain, A., Salahuddin, A. Z. M., "Experimental cross section of the $^{174}Yb(n,\gamma)^{175}Yb$ reaction at 0.0334 eV energy using monochromatic neutrons from a TRIGA nuclear reactor" International Conference on Physics-2018, 08-10 March, 2018, University of Dhaka, Dhaka, Bangladesh.

[2] Zaved, M.M., Islam, M. A., "Application of Nuclear Research Reactor for Nuclear Data Measurement" Forum for Nuclear Cooperation in ASIA (FNCA) Workshop on Research Reactor Utilization, 22-25 October, 2018, Osaka, Japan.

[3] Zaved, M.M. and Islam, M. A., "Experimental cross sections of the $^{55}Mn(n,\gamma)^{56}Mn$ reaction at new energies of 0.0334 eV and 0.0536 eV" International Conference on Physics for Sustainable Development and Technology (ICPSDT)-2019, 18-19 December, Chittagong University of Engineering and Technology, Chittagong, Bangladesh.